Cellular Origin, Tumor Progression, and Pathogenic Mechanisms of Cutaneous Neurofibromas Revealed by Mice with Nf1 Knockout in Boundary Cap Cells

Katarzyna J Radomska, Fanny Coulpier, Aurelie Gresset, Alain Schmitt, Amal Debbiche, Sophie Lemoine, Pierre Wolkenstein, Jean-Michel Vallat, Patrick Charnay, Piotr Topilko

To cite this version:

Katarzyna J Radomska, Fanny Coulpier, Aurelie Gresset, Alain Schmitt, Amal Debbiche, et al.. Cellular Origin, Tumor Progression, and Pathogenic Mechanisms of Cutaneous Neurofibromas Revealed by Mice with Nf1 Knockout in Boundary Cap Cells. Cancer Discovery, In press, 9 (1), pp.130-147. 10.1158/2159-8290.CD-18-0156 . hal-03822481

HAL Id: hal-03822481
https://hal.science/hal-03822481

Submitted on 20 Oct 2022

HAL is a multi-disciplinary open access archive for the deposit and dissemination of scientific research documents, whether they are published or not. The documents may come from teaching and research institutions in France or abroad, or from public or private research centers.

L'archive ouverte pluridisciplinaire **HAL**, est destinée au dépôt et à la diffusion de documents scientifiques de niveau recherche, publiés ou non, émanant des établissements d'enseignement et de recherche français ou étrangers, des laboratoires publics ou privés.

Cellular origin, tumour progression and pathogenic mechanisms of cutaneous neurofibromas revealed by mice with *Nf1* knockout in boundary cap cells

Katarzyna J Radomska[1], Fanny Coulpier[1], Aurelie Gresset[1], Alain Schmitt[2], Amal Debbiche[1], Sophie Lemoine[3], Pierre Wolkenstein[4], Jean-Michel Vallat[5], Patrick Charnay[1,*] and Piotr Topilko[1,6,*]

[1]*Ecole Normale Supérieure, PSL Research University, CNRS, Inserm, Institut de Biologie de l'Ecole normale supérieure (IBENS), 46 rue d'Ulm, F-75005 Paris, France*

[2]*Institut Cochin, Inserm, CNRS, Université Paris Descartes, Paris, France*

[3]*Genomic facility, Ecole normale supérieure, PSL Research University, CNRS, Inserm, Institut de Biologie de l'Ecole normale supérieure (IBENS), 46 rue d'Ulm, F-75005 Paris, France*

[4]*Département de Dermatologie, Centre de Référence des Neurofibromatoses, Hôpital Henri-Mondor, AP-HP, Créteil, France.*

[5]*National Reference Centre "Rare Peripheral Neuropathies" Department of Neurology, Centre Hospitalier Universitaire de Limoges, 87042 Limoges, France*

[6]*Lead contact*

[*]*Correspondence should be addressed to: patrick.charnay@ens.fr or topilko@biologie.ens.fr*

Running title: Origin and development of cutaneous neurofibromas

Keywords: *NF1*, *Prss56*, boundary caps, Schwann cells, neurofibroma

Downloaded from http://aacrjournals.org/cancerdiscovery/article-pdf/doi/10.1158/2159-8290.CD-18-0156/2929956/2159-8290_cd-18-0156v1.pdf by guest on 20 October 2022

DECLARATION OF INTERESTS

The authors declare no competing interests.

Downloaded from http://aacrjournals.org/cancerdiscovery/article-pdf/doi/10.1158/2159-8290.CD-18-0156/2929956/2159-8290_cd-18-0156v1.pdf by guest on 20 October 2022

SUMMARY

Patients carrying an inactive *NF1* allele develop tumours of Schwann cell origin called neurofibromas (NFs). Genetically engineered mouse models have significantly enriched our understanding of plexiform forms of NFs (pNFs). However, this has not been the case for cutaneous neurofibromas (cNFs), observed in all NF1 patients, as no previous model recapitulates their development. Here, we show that conditional *Nf1* inactivation in Prss56-positive boundary cap cells leads to bona fide pNFs and cNFs. This work identifies subepidermal glia as a likely candidate for the cellular origin of cNFs, and provides insights on disease mechanisms, revealing a long, multistep pathological process in which inflammation-related signals play pivotal role. This new mouse model is an important asset for future clinical and therapeutic investigations of NF1-associated neurofibromas.

Downloaded from http://aacrjournals.org/cancerdiscovery/article-pdf/doi/10.1158/2159-8290.CD-18-0156/2929956/2159-8290_cd-18-0156v1.pdf by guest on 20 October 2022

SIGNIFICANCE

Patients affected by NF1 develop numerous cutaneous neurofibromas (cNFs). We present a mouse model that faithfully recapitulates cNFs, identify a candidate cell type at their origin, analyze the steps involved in their formation and show that their development is dramatically accelerated by skin injury. These findings have important clinical/therapeutic implications.

Downloaded from http://aacrjournals.org/cancerdiscovery/article-pdf/doi/10.1158/2159-8290.CD-18-0156/2929956/2159-8290_cd-18-0156v1.pdf by guest on 20 October 2022

INTRODUCTION

Neurofibromatosis type 1 (NF1) is a common human genetic disorder caused by heterozygous loss-of-function of the tumour suppressor gene *NF1*, encoding neurofibromin 1. It predisposes patients to develop benign nerve sheath tumours, termed neurofibromas (NFs). While about 20% of NF1 patients suffer from plexiform NFs (pNFs) along peripheral nerves tracts, with significantly higher incidence at nerve roots, all of them develop cutaneous NFs (cNFs) localised at nerve terminals in the skin (1). cNFs typically appear at puberty and tend to increase in number throughout life, so that they may reach thousands. Although of benign character, these tumours can be disfiguring and painful, thus significantly affecting quality of life. All NFs are composed of a mixture of Schwann cells (SCs) with other nerve fibre elements, such as axons, fibroblasts, mastocytes, macrophages and endothelial cells. Despite this marked cellular heterogeneity, NFs are known to arise from cells belonging to the SC lineage in which the remaining functional copy of *NF1* is mutated, resulting in complete *NF1* loss-of-function and permanent hyperactivation of the Ras proto-oncogene and its downstream effectors (1). However, the specific cell type within the SC lineage in which the second-hit mutation occurs is still controversial. Although non-myelinating SCs (nmSC) were initially considered the primary pathogenic target, several recent studies suggest that at least pNFs arise as a result of *Nf1* mutation at earlier stages in the SC lineage, possibly as early as neural crest stem cells (2).

Recently, significant efforts have been made to develop genetically engineered mouse (GEM) models to study Nf1-associated NFs (2). These genetic tools have allowed major advances in the understanding of the mechanisms implicated in pNF formation. However, as none of these models recapitulate the development of cNFs, their origin and pathogenic

Downloaded from http://aacrjournals.org/cancerdiscovery/article-pdf/doi/10.1158/2159-8290.CD-18-0156/2929956/2159-8290_cd-18-0156v1.pdf by guest on 20 October 2022

mechanisms remain largely unknown. There is therefore an urgent need to develop new animal models that recapitulate cNFs and allow their experimental analysis.

As possible candidates for the cells at the origin of paraspinal pNFs (ppNFs), neural crest-derived boundary cap (BC) cells, which are transiently located at the embryonic nerve root entry/exit zone, have attracted particular attention. Using the *Krox20/Egr2* gene as a marker for BC cells, we have demonstrated that *Krox20*-expressing BC cells give rise to the entire SC component of the nerve roots, precisely where ppNFs develop (3). Furthermore, conditional inactivation of *Nf1* in *Krox20*-expressing cells gives rise to ppNFs, but not cNFs (4). This suggests that *Nf1* inactivation in the Krox20-positive BC cell lineage leads to pNFs and that cNFs do not originate from these cells. Recently, we have identified another BC cell marker, *Prss56*, and developed a mutant allele, $Prss56^{Cre}$, in which the Cre recombinase coding sequence is inserted into the locus (5). *In vivo* fate mapping analyses with this allele indicated that BC derivatives migrate into the nerve roots and, along peripheral nerves, into nerve terminals in the skin, precisely the two locations where NFs are observed (6). These observations led us to hypothesize that the lineage of *Prss56*-expressing BC cells might be the target for *Nf1* mutation in both plexiform and cutaneous forms of NFs.

In the present study, we have generated and characterised mice carrying bi-allelic *Nf1* deletions in *Prss56*-expressing BC cells and their progeny, by introducing $Prss56^{Cre}$ and the Cre-activable reporter $R26^{tdTom}$ alleles into *Nf1*-floxed backgrounds ($Nf1^{fl/fl}$ or $Nf1^{fl/-}$), susceptible to loss-of-function upon Cre recombination. This approach allows conditional deletion of *Nf1* in *Prss56*-expressing BC cells and *in vivo* tracing of mutant cells due to permanent expression of the fluorescent reporter. We found that both types of mutants develop numerous cNFs and pNFs. As inactivation of *Nf1* in the peripheral nervous system (PNS) is restricted to *Prss56*-expressing BC cells and their derivatives, this population is clearly directly involved in the development of NFs. Our model allows a detailed analysis of

Downloaded from http://aacrjournals.org/cancerdiscovery/article-pdf/doi/10.1158/2159-8290.CD-18-0156/2929956/2159-8290_cd-18-0156v1.pdf by guest on 20 October 2022

cNF development, leading to critical observations on the aetiology, progression and properties of the disease that are of prime importance for clinical and therapeutic applications.

Downloaded from http://aacrjournals.org/cancerdiscovery/article-pdf/doi/10.1158/2159-8290.CD-18-0156/2929956/2159-8290_cd-18-0156v1.pdf by guest on 20 October 2022

RESULTS

Prss56-expressing BC cells give rise to glial and non-glial derivatives in nerve roots and skin nerve terminals

We have previously shown that derivatives of *Prss56*-expressing BC cells migrate into nerve roots and nerve terminals in the skin (6). Here, using $Prss56^{Cre},R26^{tdTom}$ mice, we present a detailed characterisation of tdTomato (TOM)-traced cells in these two structures. As expression of *Prss56* was never detected in nerve roots nor in the skin, we consider that all traced cells in these tissues correspond to BC derivatives ((6), and Fig. S1A). Consistent with our previous report (6), numerous traced cells were present along the adult dorsal and ventral nerve roots and in the dorsal root ganglia (DRG), but there were only a few in the proximal segment of the spinal nerves (Fig. 1A). In the trunk of the sciatic nerve, TOM staining was absent from SCs (S100-positive; S100+) and remained restricted to a small subset of axons (TUJ1+) (Fig. S1B). We performed immunohistochemical (IHC) analyses in the nerve roots with SC marker S100 and neural crest lineage marker SOX10 (Fig. 1B-D). All traced cells were derived from the neural crest, whereas only a subset of the SOX10+ population was traced (Fig. 1C). Quantification in cervical dorsal nerve roots indicated that 76.1 ± 10.2% (mean ± SD) of the SOX10+ cells originated from *Prss56*-expressing BC cells. Most traced cells were S100+ and correspond to myelinating (mSC) and non-myelinating (nmSC) SCs, according to their morphology and organisation with respect to axons. The level of S100 expression was much weaker in nmSCs than mSCs (Fig. 1B, D).

In addition to SCs, we observed a small subset of TOM+ endoneurial cells that lacked S100-immunoreactivity (Fig. 1B), possibly corresponding to neural crest-derived endoneurial fibroblasts (eFBs) (7). To explore this possibility, we immunolabelled adult nerve roots with TOM, a generic fibroblast marker PDGFRα and CD34, recently identified as a putative eFB

Downloaded from http://aacrjournals.org/cancerdiscovery/article-pdf/doi/10.1158/2159-8290.CD-18-0156/2929956/2159-8290_cd-18-0156v1.pdf by guest on 20 October 2022

marker in human and rat peripheral nerves (8). Whereas numerous cells expressing these markers were observed in the endoneurial space, no overlap with TOM labelling was observed. (Fig. S1C, D). Further studies will therefore be required to characterise the identity of this TOM+/S100- population. Finally, we have never observed TOM+ perineurial fibroblasts (Fig. 1B and Fig. S1E).

In the adult skin, traced cells were found in the dermis (Fig. 1E) and hypodermis (subcutis) (Fig. 1F) but were absent from the epidermis (Fig. 1G). In the dermis, they showed a highly heterogeneous distribution, with patches aligned with some, but not all nerves and nerve terminals (Fig. 1E, G). IHC analysis with S100 revealed that most of these cells correspond to nmSCs (Fig. 1G). Nevertheless, we also observed a few traced mSCs (S100+/MBP+) enwrapping rare large-diameter fibres, mainly located in the lower dermis or innervating hair follicles (Fig. S1F). Dermal traced nmSCs exhibited broad heterogeneity and could be classified into four categories: (i) typical nerve-associated nmSCs unsheathing small-calibre axons (Remak SCs; Fig. 1G), (ii) hair follicle-associated glia unsheathing lanceolate nerve endings (Fig. 1G, H) (iii) glia associated with the arrector pili muscle (Fig. 1G, I), and (iv) terminal glia associated with nociceptive free nerve endings (Fig. 1G, J and Fig. S1G). This later population, residing directly beneath the epidermis (thus further referred to as subepidermal SCs), is characterised by a complex multipolar morphology and remains largely uncharacterised, although it has been identified in the human hairy skin (9) (10). Analysis of large skin fragments also revealed the presence of pigmented TOM+ and KIT+ melanocytes, in a subset of hair follicle bulbs (Fig. 1K, K' and Fig. S1H, H'). Finally, while BC derivatives are absent from the trunk of peripheral nerves, they populate subcutaneous nerve branches, where they correspond to a subset of mSCs, nmSCs and eFBs (Fig. 1F and (6)).

Downloaded from http://aacrjournals.org/cancerdiscovery/article-pdf/doi/10.1158/2159-8290.CD-18-0156/2929956/2159-8290_cd-18-0156v1.pdf by guest on 20 October 2022

Together, our observations indicate that *Prss56*-expressing BC cells participate in the development of nerve roots and cutaneous/subcutaneous innervation as a source of glial and non-glial derivatives.

Conditional *Nf1* knockout in BC cells leads to skin lesions and progressive limb paralysis

Since BC derivatives populate nerve roots and nerve terminals in the skin, two highly favoured sites for NF development, we explored whether *Nf1* knockout in *Prss56*-expressing BC cells was sufficient to promote formation of NFs in the mouse. We transferred the $Prss56^{Cre}$,$R26^{tdTom}$ alleles into $Nf1^{flox/-}$ or $Nf1^{floxflox}$ backgrounds to generate $Prss56^{Cre}$,$R26^{tdTom}$,$Nf1^{flox/-}$ and $Prss56^{Cre}$,$R26^{tdTom}$,$Nf1^{flox/flox}$ progeny, collectively referred to as *Nf1*-KO mutants. These mutant animals should carry bi-allelic *Nf1* knockout in BC cells and their derivatives, in a *Nf1* heterozygous or wild-type background, respectively. As *Prss56* expression is restricted to BC cells between embryonic day (E) E11 and E13 and is absent from any other component of the PNS, recombination at the *Nf1* locus should occur during this period (5). Moreover, as TOM is activated in parallel to *Nf1* inactivation, this should allow identification of the cells carrying the *Nf1* knockout. The efficiency of Cre-mediated recombination at the *Nf1* locus was evaluated using semi-quantitative RT-PCR. No *Nf1* expression was observed in *Nf1* mutant cells, demonstrating efficient recombination (Fig. S1A).

The use of the two genetic backgrounds ($Nf1^{flox/-}$ or $Nf1^{flox/flox}$) for the analysis of the phenotypes associated with the targeted mutation is important, because in some of the existing *Nf1* GEM models, tumourigenicity requires inactivation of both *Nf1* alleles in the cells that become neoplastic, along with inactivation of one allele in the tumour environment (4). As controls (CTRL), we used $Prss56^{Cre}$,$R26^{tdTom}$,$Nf1^{flox/+}$ littermates, which carry only a

Downloaded from http://aacrjournals.org/cancerdiscovery/article-pdf/doi/10.1158/2159-8290.CD-18-0156/2929956/2159-8290_cd-18-0156v1.pdf by guest on 20 October 2022

heterozygous *Nf1* inactivation in the BC cell lineage in a wild-type background. Control animals did not develop any abnormalities and were phenotypically indistinguishable from wild-type animals. Both types of *Nf1*-KO mutants were born at the expected Mendelian frequency and all developed identical symptoms, at 10.0 ± 4.5 months and 13.1 ± 3.9 months (mean ± SD) of age for $Nf1^{flox/-}$ and $Nf1^{flox/flox}$ backgrounds, respectively (Table S1). The symptoms included lethargy and numerous skin lesions, mainly localised on the neck, and were often accompanied by progressive limb paralysis. Skin lesions were typically accompanied by pruritus that required the sacrifice of the animals. Gross anatomical-pathological analysis of *Nf1*-KO mice revealed enlarged nerve roots/DRGs, often accompanied by tissue masses compressing the spinal cord at the cervico-thoracic level. In subsequent analyses, as the phenotypes in $Nf1^{flox/-}$ and $Nf1^{flox/flox}$ backgrounds appeared to be similar apart from the mean age of appearance, animals from both backgrounds were used interchangeably, except when explicitly indicated.

BC-derived non-myelinating Schwann cells constitute the major pathogenic cell type in plexiform neurofibroma

Gross dissection of *Nf1*-KO mutant spinal cord with the attached nerve roots revealed the presence of tumours that are largely TOM+, localised at the thoracic and/or cervical nerve roots (Fig. 2A-C). All remaining nerve roots showed signs of marked hyperplasia (Fig. 2A-C). The number of tumours varied from 1 to 4 and often affected contralateral sides. Severe spinal cord compression was frequent and likely accounted for the observed paralysis (Fig. 2C, D). Paraspinal lesions contained abnormal accumulations of disorganised, slender TOM+ cells that expressed low levels or no S100, likely corresponding nmSCs (Fig. 2E-G''). In the mutants, unlike controls, most TOM+ cells coexpressed SOX2, a marker of precursor/immature SCs (Fig. S2A-B'). In contrast, TOM+ mSCs, enwrapping large-calibre

Downloaded from http://aacrjournals.org/cancerdiscovery/article-pdf/doi/10.1158/2159-8290.CD-18-0156/2929956/2159-8290_cd-18-0156v1.pdf by guest on 20 October 2022

axons, expressed high levels of S100 and showed no obvious abnormalities (Fig. 2E-G''). We also observed increased infusion of KIT+ mastocytes and IBA1+ macrophages (both non-traced), which are always detected in human pNFs (Fig. S2C-F'). Ultrastructure analysis of paraspinal tumours revealed a substantial expansion of an interstitial compartment filled with collagen-rich extracellular matrix, and accumulation of abnormal Remak bundles (Fig. 2H-K). Mutant nmSCs (identified by continuous basal lamina) showed profound morphological abnormalities, including partial or complete dissociation from axons, and extension of numerous cytoplasmic protrusions surrounding collagen fibrils or myelinated fibres (Fig. 2I-K).

In addition, subcutaneous nerves containing traced BC derivatives were markedly enlarged, and localised enlargements (ballooning) were often observed beneath the skin lesions (Fig. 2L). Subcutaneous lesions were very similar to paraspinal tumours in their histology and ultrastructure (Fig. 2M-P), and contained large numbers of traced, S100+ nmSCs with disrupted morphologies and axonal interactions, intermixed with numerous non-traced, PDGFRα+ fibroblasts. Fibroblasts present in the peripheral part of a tumour had typical characteristics of perineurial fibroblasts, such as patchy basal lamina and the presence of pinocytic vesicles (Fig. S2G). However, unlike the control nerves, where perineurial cells form a multilayered, tightly compacted protective sheath, the perineurial compartment of the *Nf1*-KO nerves appeared much thicker and contained a high number of loosely organised fibroblasts intermingled with numerous SC processes and large amounts of collagen (Fig. 2O, P). Despite these abnormalities, nerve integrity seemed to be preserved. Finally, as in paraspinal lesions, there was an increased influx of mastocytes and an even more pronounced infiltration of macrophages in the tumour masses (Fig. S2H, H').

Downloaded from http://aacrjournals.org/cancerdiscovery/article-pdf/doi/10.1158/2159-8290.CD-18-0156/2929956/2159-8290_cd-18-0156v1.pdf by guest on 20 October 2022

Together, our observations support the previously proposed role of BC-derived nmSCs in the formation of ppNFs and a similar involvement in the development of subcutaneous tumours.

Downloaded from http://aacrjournals.org/cancerdiscovery/article-pdf/doi/10.1158/2159-8290.CD-18-0156/2929956/2159-8290_cd-18-0156v1.pdf by guest on 20 October 2022

***Nf1* inactivation in Prss56-positive cells leads to the development of diffuse cutaneous neurofibromas**

In *Nf1*-KO mice, the first macroscopically detectable cutaneous symptoms were areas of hair thinning on the neck, which rapidly evolved into pruritus (Fig. 3A, B). After shaving the hair, we frequently observed additional smaller lesions (with or without scabs) containing well-circumscribed, dense aggregates of traced cells (Fig. 3B). Such dense clusters of TOM+ cells were never observed in control skin. Although affected skin regions were significantly thicker than non-affected skin from the same individual, their basic architecture, including integrity of hair follicles, remained preserved. IHC analyses of lesioned areas indicate that (i) the diffuse accumulation of traced cells is restricted to the dermis; (ii) traced cells correspond to S100+ nmSCs. However, the level of S100 was significantly lower than in rare mSCs. These nmSCs appear highly disorganised and extend numerous slender cytoplasmic processes (Fig. 3C-D’). Their SC identity is further supported by expression of other known nmSC/immature SC markers, including p75NTR, NCAM and L1, as well as SOX2 (Fig. S3A-D); (iii) mutant nmSCs express high levels of phosphorylated Mitogen-Activated Protein Kinase (ERK1/2), a downstream effector of Ras (Fig. S3E); (iv) numerous non-traced KIT+ mastocytes, IBA1+ macrophages and PECAM+ blood vessels infiltrate the lesion (Fig. 3E-F’ and Fig. S3F); (v) the dermal fibroblast population (non-traced and defined by PDGFRα expression) is drastically enlarged (Fig. 3G, G') and accompanied by heavy deposition of collagen (Fig. 3H); (vi) both traced and non-traced pigmented cells, presumably melanocytes, are often concentrated in extrafollicular dermis within the lesion (Fig. 3I).

Ultrastructural analysis of the *Nf1*-KO skin lesions confirmed that numerous nmSCs with severely affected morphologies are present in the dermis. These SCs form a dense network of cytoplasmic extensions that often enwrap isolated axons and/or are devoid of axonal contact, and enclose clusters of collagen fibrils, forming apparent collagen pockets (Fig. 3J, K). Immuno-electron microscopy confirmed that most of these cells express TOM and correspond to mutant nmSCs (Fig. 3K). Finally, numerous fibroblasts (identified by morphology and the absence of basal lamina) and collagen fibres were observed at the level of the lesions (Fig. S3G). Since endoneurial and perineurial fibroblasts are rare or absent in the dermis, we assume that this accumulation of fibroblasts mainly corresponds to recruitment and/or proliferation of mesodermally-derived dermal population (non-traced). Lack of basal lamina and pinocytic vesicles, typical characteristics of perineurial fibroblasts, further supports their dermal identity. While in control skin, dermal fibroblasts are rare, of round shape, with few ribosomes and poorly developed endoplasmic reticulum (ER), in the *Nf1*-KO mutant dermis, they often form long cytoplasmic extensions with or without collagen pockets and contain numerous ribosomes and highly developed ER (Fig. S3G-I), supporting their engagement in the active synthesis of collagen. Finally, in addition to infiltration by mastocytes and macrophages, ultrastructural analysis revealed accumulations of polymorphonuclear neutrophils, which were only sporadically observed in control skin (Fig. S3J).

In conclusion, all morphological, cellular and molecular characteristics associated with the cutaneous lesions are highly similar to those of diffuse human cNFs (11). These data

Downloaded from http://aacrjournals.org/cancerdiscovery/article-pdf/doi/10.1158/2159-8290.CD-18-0156/2929956/2159-8290_cd-18-0156v1.pdf by guest on 20 October 2022

indicate that the loss of *Nf1* in dermal BC derivatives is sufficient to promote development of cNFs. This is correlated with activation of the ERK signalling pathway in mutant SCs.

Development of cNFs involves progressive alterations of the dermis

Although NF1 patients develop cNFs during adulthood after a long asymptomatic period, it is unclear whether these tumours appear suddenly in the adult skin or whether they slowly evolve from micro-tumoural loci already present at younger ages. To investigate this issue, we compared the skin of *Nf1*-KO mice and control littermates from embryonic day E13.5, when the first traced BC derivatives settle in the skin, until 6 months after birth, when most mutants do not show obvious cutaneous manifestations. For this study, we used only $Prss56^{Cre},R26^{tdTom},Nf1^{flox/-}$ mutants which, similar to NF1 patients, harbour heterozygous germline *Nf1* mutation along with homozygous *Nf1* knockout in the SC lineage. The inactivation of *Nf1* in BC cells around E11 did not affect the migration of BC-derived progenitors along the nerves to the skin nor the number of traced SC precursors or immature SCs in the embryonic skin (Fig. S4A-F). This suggests that the early specification and migration of the SC lineage is not affected in the absence of *Nf1*. At birth, however, the number of traced SCs in *Nf1*-KO was nearly double that in control skin (Fig. 4A-C), although all mutant SCs remained in contact with axons and did not show any morphological abnormalities. Intraperitoneal 5-ethynyl-2’-deoxyuridine (EdU) injection into pregnant females at E18.5, followed by analysis of newborn skin, revealed a small but significant ($p = 0.036$) increase in the proportion of proliferating SCs (EdU+/TOM+) in *Nf1*-KO (22.6 ± 1.37%) compared to control animals (18.19 ± 1.89%, mean ± SEM). Slow SC proliferation is later maintained in cNFs, as immunolabelling of cNFs from 10-month-old *Nf1*-KO mutants against the mitotic marker phospho-histone-H3 (PHH3) indicates that a small proportion of traced cells undergo mitosis (Fig. S3K). This is in line with clinical observations

Downloaded from http://aacrjournals.org/cancerdiscovery/article-pdf/doi/10.1158/2159-8290.CD-18-0156/2929956/2159-8290_cd-18-0156v1.pdf by guest on 20 October 2022

demonstrating rare mitoses in human NFs (12). Overall, our data suggests that inactivation of *Nf1* provides a small proliferative advantage to neonatal mutant SCs.

As BC derivatives include a subset of skin melanocytes, we compared the number of cells co-expressing TOM and the melanocyte lineage marker TRP2 between *Nf1*-KO and control, newborn animals. While we observed no difference in the number of traced melanoblasts within the hair follicles, the extrafollicular (dermal) fraction was substantially increased in *Nf1*-KO skin (Fig. 4D-F). Interestingly, there was already enhanced melanocytogenesis in embryonic mutant skin at E15.5 (Fig. S4G-L). At P9, when melanoblast migration into developing hair follicles is complete in control skin, numerous double-positive (TOM+/TRP2+) cells were still observed in the mutant dermis. Conversely, there was no difference in the numbers of traced follicular melanocytes (Fig. S4M), suggesting a selective expansion of the extrafollicular melanocyte fraction in the mutant.

We next investigated whether the elevated SC content in mutant newborn skin is accompanied by modifications of the other cell types. Although *Nf1*-KO skin had a slight (1.1-fold) elevation in the number of KIT+ mastocytes compared to controls (Fig. 4G), the densities of PDGFRα+ fibroblasts (Fig. 4H, I) and of IBA1+ macrophages (Fig. 4J) were comparable between the two groups.

Analysis of the postnatal back skin between P0 and 3 months of age revealed a further progressive increase in the numbers of TOM+ SCs in *Nf1*-KO mutants compared to controls (Fig. 4K-M and Fig. S4N). Although at three months, most traced SCs were still well-aligned with axons, many appeared hypertrophic and extended numerous cytoplasmic protrusions that detached from axons (Fig. 4N-O''). In some cases, we observed an entire SC soma "escaping" from the nerve bundle (Fig. 4O''). These abnormal morphologies preferentially occurred in the upper dermis (Fig. S5A-D). In addition, we observed a dramatic increase in the density of dermal fibroblasts, as revealed by labelling for PDGFRα and increased density

Downloaded from http://aacrjournals.org/cancerdiscovery/article-pdf/doi/10.1158/2159-8290.CD-18-0156/2929956/2159-8290_cd-18-0156v1.pdf by guest on 20 October 2022

of nuclear staining (Fig. 4P, Q). However, as in the newborn skin, the number of mastocytes was only slightly (1.4-fold) higher in *Nf1*-KO dermis than in controls (Fig. 4R), whereas the density of macrophages was unaffected (Fig. S4O, P).

It is surprising that despite their increased number, mutant SCs mostly remain in contact with axons for up to 3 months. This observation raises the possibility of an increase in the density of cutaneous innervation to cope with elevated SC numbers. To examine innervation density, we performed whole-mount immunostaining of the 3-month-old *Nf1*-KO and control skin with antibodies against TOM and the pan-axonal marker ß-III-tubulin (TUJ1). The density of innervation appeared higher in the regions of *Nf1*-KO skin corresponding to patches of traced SCs as compared to controls or regions of mutant skin poor in traced cells (Fig. S5E-G). This suggests that enhanced local innervation in the mutant skin is linked to SC hyperplasia. To investigate if enhanced innervation might result from increased sensory DRG neurogenesis, we compared the numbers of traced sensory neurons in *Nf1*-KO mutant and control newborn DRGs from the same A-P level (Fig. S5H). There was no significant difference in the number of traced sensory neurons, suggesting that enhanced innervation is rather due to branching of nerve terminals in the mutant dermis.

We next analysed the skin of 6-month-old *Nf1*-KO mice, which still did not show any visually detectable abnormalities. However, numerous microscopic lumps were detected upon tactile examination. Histological analysis of the skin revealed SC hyperplasia along with the presence (over the entire back skin) of multiple small (up to 1 mm) aggregates of disorganised nmSCs, positive for TOM and S100 (Fig. 5A-C), which were intermixed with numerous non-traced fibroblasts, mastocytes, macrophages and polymorphonuclear neutrophils, all present in typical cNFs. Quantification of distinct cell populations was performed by electron microscopy (Fig. 5D). Interestingly, the presence of inflammation-related cells, such as neutrophils, mastocytes and macrophages in these micro-lesions suggests these cell types are

Downloaded from http://aacrjournals.org/cancerdiscovery/article-pdf/doi/10.1158/2159-8290.CD-18-0156/2929956/2159-8290_cd-18-0156v1.pdf by guest on 20 October 2022

involved in the development and/or progression of tumours rather than being a simple consequence of pruritus-related inflammation. Ultrastructural characteristics of nmSCs in the micro-lesions were also typical of classical cNFs and included abnormal extension of cytoplasmic processes that enclosed isolated axons and/or groups of collagen fibrils, or were devoid of axonal contact (Fig. 5E, F). Whole-mount immunostaining of the mutant dermis confirmed accumulation of traced SCs with profound morphological aberrations (Fig. 5G-H'). SC hypertrophy in the upper dermis was far more severe than in 3-month-old mutants, and some cells seemed to lose contact with axons. In the lower dermis, most mutant SCs had detached from axons and extended multiple filipodia-like structures. Together these data indicate that the micro-lesions, apart from their size, share essential characteristics with bona fide cNFs and consequently, we refer to them as micro-cNFs.

Ultrastructural examination of dermal innervation also revealed that intact Remak bundles, containing small groups of tightly packed axons, were extremely rare in the mutant dermis. Instead, we commonly observed numerous isolated axons that were separated by large quantities of collagen and individually ensheathed by small fragments of SC cytoplasm (Fig. 5F). This suggests decompaction of nerve bundles. Moreover, we observed a 2-fold increase in axon numbers between control and *Nf1*-KO dermis (Fig. 5D). Immunolabelling with CGRP, a marker of peptidergic nociceptive neurons (13) further supported an increased density of dermal innervation in micro-cNFs compared to control dermis (Fig. S5I-L). Overall, these data point toward a marked decompaction of nerve bundles combined with increased branching of axon terminals in the mutant dermis.

If micro-cNFs constitute a precursor stage of full-blown tumours, it would be expected that the number of tumours arising in older individuals should be much larger than what was actually observed (typically up to a few well-demarcated lesions per mutant at the cervical or cervico-thoracic level). As mutant mice had to be sacrificed as soon as pruritic lesions

Downloaded from http://aacrjournals.org/cancerdiscovery/article-pdf/doi/10.1158/2159-8290.CD-18-0156/2929956/2159-8290_cd-18-0156v1.pdf by guest on 20 October 2022

appeared, it is likely that most of the developing tumours did not have enough time to reach a macroscopically detectable stage. Indeed, this idea is supported by the observation of a unique *Nf1*-KO individual that survived until 20 months of age without developing pruritus. In this case, dozens of raised skin bumps containing dense clusters of traced cells were observed all over the back skin. Analysis of their cellular composition with the set of markers described above confirmed their cNF identity (Fig. S3L-N). This strongly supports the hypothesis that many of the micro-cNFs observed in the 6-month-old skin could evolve into full-blown diffuse cNFs in older animals.

Downloaded from http://aacrjournals.org/cancerdiscovery/article-pdf/doi/10.1158/2159-8290.CD-18-0156/2929956/2159-8290_cd-18-0156v1.pdf by guest on 20 October 2022

Skin injury accelerates the development of cNFs

In NF1 patients, surgical and laser ablation of cutaneous tumours are routinely used for tumour resection. However, several case reports suggest that skin injury (trauma) might promote development of additional cNFs (14). To test whether an injury favors the appearance of tumours, small skin incisions were made at the thoracic level on 3-month-old *Nf1*-KO mutants (n=6) and control individuals (n=4). These animals were sacrificed at 10 months of age and their skin was analysed and compared with that of uninjured age-matched *Nf1*-KO mutants (n=6). All injured *Nf1*-KO mutants developed large, mostly non-pruritic lesions at the site of injury (Fig. 6A-a). Furthermore, all injured mutants also developed numerous, smaller (≤ 5 mm), well-demarcated lesions all over the back skin (Fig. 6A-d). Both types of lesions, at the injury site or distant from it, contained dense accumulations of TOM+ cells (Fig. 6A-b, d', f, g). Thoracic and lumbar lesions were histologically identical (except for their size) and corresponded to typical diffuse cNFs (Fig. 6A-f, g, i-k). No abnormalities in the distribution or densities of traced cells were ever observed in injured control animals (Fig. 6A-c). Moreover, we did not observe any morphologically visible skin lesions at the thoracic or lumbar level in 10-month-old uninjured *Nf1*-KO mutants (Fig. 6A-e). The accumulation of traced cells in this region was limited and corresponded to micro-cNFs (Fig. 6A-e', h). Furthermore, in our original *Nf1*-KO cohort (Table S1), morphologically visible lesions were rare at the thoracic level (4 animals out of 26) and only found in aging individuals (17.5 ± 3.6 months). Finally, while the thickness of the skin in the uninjured mutants in the lumbar region was typical of early stage micro-NFs (Fig. 6A-h), it was increased in the same region in injured mutants (Fig. 6A-g), consistent with cNF stage. Skin thickness reached an unprecedented level in the thoracic region of the injured mutants, with a dramatic expansion of the number of traced cells (Fig. 6A-f).

Wound healing following skin injury is a highly dynamic process that involves soluble mediators, extracellular matrix components, resident cells, and infiltrating leukocytes, which differentially participate in three sequential phases: inflammation, proliferation, and remodeling (15). Initially, neutrophils accumulate in wound sites, followed by a large influx of macrophages that augment inflammatory response. Recent studies highlighted the role of nerves and SCs as pivotal elements promoting skin repair (16). As soon as 2 days after injury, SCs detach from sectioned nerves, proliferate and begin to invade the wound bed, where they support extracellular matrix remodeling via paracrine signaling. This delamination is transient as 2 weeks later many SCs at the site of injury are associated with nerves. To investigate the impact of skin injury on BC-derived *Nf1*-KO SCs, we analyzed TOM+ cells at 2, 4, 7 and 14 day post-injury (dpi) in 3-month-old control (*Prss56*^{Cre}*, R26*^{tdTom}) and *Nf1*-KO animals (Fig. 6B). During the peak of the inflammation phase (2-4 dpi), traced *Nf1*-KO and control SCs from the damaged nerves were similarly distributed into the wound bed (Fig. 6B-a-d). However, by day 7, the number of *Nf1*-KO SCs drastically increased as compared to control SCs, and this phenomenon was even more pronounced at 14 dpi (Fig. 6B-e-h). Rapid expansion of the mutant SC lineage was also supported by the observation that the majority of *Nf1*-KO SCs expressed the proliferation marker PH3 at 7dpi (inset in Fig. 6B-f). In addition,

Downloaded from http://aacrjournals.org/cancerdiscovery/article-pdf/doi/10.1158/2159-8290.CD-18-0156/2929956/2159-8290_cd-18-0156v1.pdf by guest on 20 October 2022

detailed analysis of 14 dpi mutant wounds revealed the presence of morphologically abnormal *Nf1*-KO SCs, similar to those observed in cNFs (Fig. 6B-h'). At this stage, numerous *Nf1*-KO SCs were still dissociated from the axons, in contrast to control SCs (Fig. 6B-g', h'). Furthermore, macrophage and fibroblast, but not mastocyte, densities were increased in *Nf1*-KO as compared to control wounds, suggesting enhanced inflammatory response in the mutant.

To identify candidate factors involved in the abnormal behavior of *Nf1*-KO SCs and their microenvironment upon injury, and possibly in the acceleration of cNF development, we analyzed the distribution of mRNAs by high throughput sequencing in wounded (14 dpi) and intact skin from *Nf1-KO* and control mice (n=3). *Prss56* mRNA was undetected across all compared samples, excluding the possibility of *de novo* activation of this gene in the skin upon injury. Among the 9627 genes found to be differentially transcribed ($p<0.05$; fold change, FC>4x) between injured and uninjured control skin, 13.4 % were upregulated and 86.6% downregulated. Among the 4112 genes differentially transcribed between injured and uninjured *Nf1*-KO skin, 34% were upregulated and 66% downregulated (Fig. 6C-a). Kyoto Encyclopedia of Genes and Genomes (KEGG) pathway enrichment analyses performed on the upregulated transcripts identified "Cytokine-cytokine receptor interaction", "ECM-receptor interaction", "Complement and coagulation cascades", "Protein digestion and absorption" and "Focal adhesion" among the top ranked pathways in injured vs uninjured skin comparisons, in both *Nf1*-KO and control (Fig. 6C-b, c and Table S2). As expected, many genes from these lists have previously been implicated in wound healing and tissue repair (17). Remarkably, similar to the wounded *Nf1*-KO skin, "Cytokine-cytokine receptor interaction" has also been reported as the most enriched pathway in mouse neurofibroma-derived SCs and macrophages (18), suggesting the involvement of similar paracrine/autocrine signaling pathways. More specifically, among the cytokines identified as significantly

Downloaded from http://aacrjournals.org/cancerdiscovery/article-pdf/doi/10.1158/2159-8290.CD-18-0156/2929956/2159-8290_cd-18-0156v1.pdf by guest on 20 October 2022

upregulated in injured vs uninjured *Nf1*-KO skin, *Ccl2* (FC=10.5x), *Ccl5* (FC=17.4x), *Ccl12* (FC=22.6x), *Cxcl5* (FC=37.2x), *Cxcl12* (FC=11.3x), *Cxcl13* (FC=7.2x), *Il1b* (FC=9.2x) and *Pf4* (FC=13.4x) have previously been reported as overexpressed in human and/or mouse neurofibromas compared to healthy nerves (18,19). Furthermore, 39% of the upregulated genes in this KEGG category were specifically activated in *Nf1*-KO and not in control animals, suggesting the existence of differences in injury-induced inflammatory response and tissue repair between mutant and control mice (Table S2). This observation is in line with the increased density of mutant SCs and macrophages observed in *Nf1*-KO wound beds. Of particular interest, *Ccl5*, which encodes a potent chemoattractant for immune effector cells, including macrophages, and has been reported as upregulated in both neurofibroma $Nf1^{-/-}$ SCs and macrophages (18), was among the genes specifically activated in *Nf1*-KO wounds. Its receptors, *Ccr5* and *Ccr1,* were upregulated in both *Nf1*-KO and control wounds, although with a higher FC in mutant (8.8x and 12.6x) than in control (4.4x and 6.7x) skin. This makes *Ccl5* an interesting candidate for being involved in early development of cNFs. *Cx3cr1* was also found specifically upregulated in *Nf1*-KO wounds (FC=5.8x). It encodes a macrophage and fibroblast chemokine receptor known to promote macrophage and fibroblast accumulation in the wound site, as well as collagen deposition (20). Furthermore, Cx3cr1-mediated signaling has recently been implicated in NF1-related optic glioma formation (21). Finally, the mRNA levels of *Ccl2,* its receptor *Ccr2* and *Ccl3*, which are also implicated in macrophage recruitment, were more strongly increased in *Nf1*-KO (10.5x, 13.2x and 23.8x) than in control (6x, 4.8x and 4.8x) skin comparisons.

Together our findings demonstrate that skin injury promotes cNF development. The injury has a rapid impact on *Nf1-KO* SC proliferation, morphology and interactions with axons. RNA-seq analysis of the skin supports the implication of inflammation-related signals in the

Downloaded from http://aacrjournals.org/cancerdiscovery/article-pdf/doi/10.1158/2159-8290.CD-18-0156/2929956/2159-8290_cd-18-0156v1.pdf by guest on 20 October 2022

acquisition of an invasive, pro-tumorigenic SC phenotype and provides several gene candidates susceptible to play key roles in this process.

Subepidermal glia are the likely cell type at the origin of cutaneous neurofibroma

It is striking that mice subjected to targeted *Nf1* inactivation in Krox20+ BC cells or Dhh+ SC precursors develop pNFs, but never diffuse cNFs (22). A likely explanation is that the BC derivatives that migrate into the skin and participate in development of cNFs do not activate these two genes. To test this hypothesis, *in vivo* fate mapping and characterisation of derivatives of either *Krox20*- or *Dhh*-expressing progenitors in the adult skin was achieved by morphological and molecular analysis of TOM+ cells from $Krox20^{Cre},R26^{tdTom}$ and $Dhh^{Cre},R26^{tdTom}$ adult animals. In $Krox20^{Cre},R26^{tdTom}$ mice, the TOM+ cells in the skin correspond to the rare S100+/MBP+ mSCs, NG2+ pericytes and previously described keratinocytes and hair follicle cells (23,24) (Fig. 7A-B''). Notably, traced nmSCs were never observed. Expression of TOM in mSCs is likely to reflect *Krox20* locus activation in mSC precursors around E15.5 (23), rather than a BC origin of these cells.

Analysis of $Dhh^{Cre},R26^{tdTom}$ adult skin revealed that a majority of SCs were traced in the hypodermis (Fig. 7C). In the dermis, TOM+ cells corresponded to various glial and non-glial derivatives (Fig. 7D-G'). However, subepidermal glia, unsheathing nociceptive fibres at the dermis/epidermis boundary and melanocytes were not traced, in stark contrast to the situation in $Prss56^{Cre},R26^{tdTom}$ skin (Fig. 7D, H, I).

Together these observations indicate that Prss56-, Krox20- and Dhh-traced populations give rise to overlapping and distinct types of glial populations in the skin (summarised in Fig. 7J). Among them, the only cell type uniquely derived from Prss56+ cells is the subepidermal glia. As diffuse cNFs do not develop upon conditional *Nf1* loss in

Downloaded from http://aacrjournals.org/cancerdiscovery/article-pdf/doi/10.1158/2159-8290.CD-18-0156/2929956/2159-8290_cd-18-0156v1.pdf by guest on 20 October 2022

Krox20- and Dhh-traced lineages, subepidermal SCs are likely to be the cell type at the origin of cutaneous neurofibromas.

Downloaded from http://aacrjournals.org/cancerdiscovery/article-pdf/doi/10.1158/2159-8290.CD-18-0156/2929956/2159-8290_cd-18-0156v1.pdf by guest on 20 October 2022

DISCUSSION

Several mouse models of NF1 have been previously developed with two major objectives: to recapitulate the various aspects of the human disease and to provide cues on the cellular origins of the different types of neurofibromas. These objectives have been so far only partially fulfilled, as diffuse cNFs are not recapitulated in these models (2). In the present study, we performed targeted inactivation of *Nf1* in Prss56-positive BC cells and observed the development of bona fide plexiform and cutaneous NFs. Comparison with previous models, together with an intrinsic tracing system, allow us to suggest a precise hypothesis on the cell type at the origin of cNFs. Furthermore, follow up of mutant animals from birth until the appearance of cNFs has allowed a detailed description of disease progression and revealed decisive steps in tumour development. Understanding these steps is likely to impact the search for therapeutic molecules against cNFs. Finally, the discovery that the skin trauma might stimulate the systemic progression of micro-cNFs into full-blown cNFs is also of clinical relevance.

The data derived from the alternative NF1 GEM models suggest that the cells at the origin of cNFs are not targeted for *Nf1* inactivation in these cases. More specifically, comparison of fate tracing performed with the Cre drivers $Prss56^{Cre}$ and Dhh^{Cre}, combined with the fact that in our model, development of cNFs appears to be initiated in the upper dermis, points to subepidermal SCs as the likely candidate for the tumour-initiating cell. Identification of specific markers for this type of glia will pave the way for direct analysis of their role in the development of cNFs in both mice and human patients. In humans, the second-hit mutation responsible for cNFs could therefore happen in subepidermal glia and/or their precursors. As our targeting system is restricted to BC cells (within PNS) and we observed the different types of NF1-associated tumours in our mutants, this work

Downloaded from http://aacrjournals.org/cancerdiscovery/article-pdf/doi/10.1158/2159-8290.CD-18-0156/2929956/2159-8290_cd-18-0156v1.pdf by guest on 20 October 2022

demonstrates that BC cells give rise to all cell types at the origin of NFs. More specifically, our tracing analyses indicate that Prss56-positive BC cells generate nerve root glia, hypodermal and dermal glia, the latter including subepidermal SCs. These three BC-derived cell types are likely to be at the origin of ppNFs, spNFs and cNFs, respectively. Finally, this work confirms that the BC cell population is heterogeneous, as previously suggested by differences in gene expression (6). Krox20-positive BC cells mostly give rise to nerve root glia ((3) and this study), and accordingly *Nf1* loss-of-function in Krox20-positive BC cells only give rise to ppNFs (4). The development of cNFs upon *Nf1* inactivation in Prss56-positive BC cells indicates that the heterogeneity of BC cells has profound physio-pathological relevance.

It is striking that, despite *Nf1* inactivation in BC cells around E11, most *Nf1*-KO animals develop cNFs only after 10 months of age. Our time-course analysis reveals that this late onset is due to a very slow but steady progression of the cutaneous disease. We have defined four stages in the development of the disease, shown in a schematic in Fig. S6. There is no indication of disease until E15.5, apart from an increased number of traced melanoblasts. At birth (Fig. S6A, stage 1), the number of traced SCs in the dermis has increased to almost the double the control number (mild hyperplasia), however with no significant morphological modifications of the cells. At three months (Fig. S6B, stage 2), the fold increase in traced SCs in *Nf1*-KO over control animals is even greater (severe hyperplasia) and their morphology is modified (hypertrophy), although most are still in contact with axons, which have undergone abnormal defasciculation and branching. This stage also involves an accumulation of fibroblasts, due to accretion and/or proliferation, and of collagen fibres presumably synthesized by these fibroblasts. At six months (Fig. S6C, stage 3), numerous micro-cNFs are present all over the back skin, which share all the characteristics of full-blown cNFs, apart from their size. They contain dense aggregates of mutant SCs that

Downloaded from http://aacrjournals.org/cancerdiscovery/article-pdf/doi/10.1158/2159-8290.CD-18-0156/2929956/2159-8290_cd-18-0156v1.pdf by guest on 20 October 2022

show altered morphologies and frequent loss of contact with the axons. These aggregates are massively infiltrated by fibroblasts, mastocytes, macrophages and neutrophils. Inflammation is therefore a major hallmark of this stage. From 12 months of age (Fig. S6D, stage 4), morphologically visible, diffuse cNFs are often associated with pruritus. On the basis of these observations, we believe that tumour progression in cNFs involves three decisive transitions: i) an increase in the level of proliferation of SCs during the late embryonic period; ii) initiation of morphological changes of SCs and the accumulation of fibroblasts between stage 1 and 2, establishing a pre-tumourous state; iii) loss of SC axonal contact and the establishment of an inflammatory process that corresponds the progression to a tumourous state, between stage 2 and 3. The transition between stage 3 and 4 may simply be a slow increase in the tumour size.

Interestingly, before stage 2, the elevation of the SCs number appears to be compensated by increased branching of nerve bundles, allowing the supernumerary SCs to maintain appropriate contacts with axons. This observation also raises the possibility that the defasciculation/branching phenomenon might actually be induced by the excess of SCs. It is possible that this putative compensatory mechanism has limitations and, when overridden, SCs can no longer interact with axons, possibly favouring a pro-tumourigenic phenotype. The branching capacity of nerve terminals in the upper dermis might be related to the absence of perineurium in this layer. Increased skin innervation might explain the skin hypersensitivity and neuropathic pain reported in approximately 10% of NF1 patients (25). If confirmed, this link could be used to predict sites of cNF development. Intriguingly, skin trauma is also accompanied by active proliferation of SCs, their dissociation from nerves and local increase of density of innervation, further supporting the impact of peripheral glia and/or inflammation on axonal branching (16).

Downloaded from http://aacrjournals.org/cancerdiscovery/article-pdf/doi/10.1158/2159-8290.CD-18-0156/2929956/2159-8290_cd-18-0156v1.pdf by guest on 20 October 2022

Presence of highly innervated microscopic neurofibromas, often associated with hair follicle apparatus was reported in clinically asymptomatic skin of NF1 patients ((26) and F. Rice, personal communication)). In our model, despite an identical cellular composition of diffuse cNFs, their association with skin adnexa cannot be firmly established due to a higher density of hair follicles present in the mouse skin. More generally, the fact that micro-cNFs in the asymptomatic patient skin might prefigure cNFs may have profound consequences in terms of therapy and raises exciting possibilities for the development of preventive treatments. For instance, reducing proliferation of SCs, preventing their hypertrophy and/or dissociation from axons, or inhibiting the recruitment and/or activity of dermal fibroblasts and immune effector cells might constitute key entry points for developing effective anti-tumour agents. Such approaches would strongly benefit from the development of non-invasive methodologies for the early detection and monitoring of micro-cNFs. The systematic development of cNFs in our mouse model makes it a powerful tool for the screening of candidate therapeutic molecules. Furthermore, the availability of the Cre-inducible fluorescent reporter that allows identification of *Nf1* mutant cells allows a continuous survey of the impact of the drug.

The similarity between patients and mice at the “pathological” level is surprising in view of their differences at the genetic level. Previous studies suggested that NF1 heterozygosity in the cellular microenvironment (particularly in mastocytes) was necessary for initiation and development of cNFs (27). However, more recent studies performed in mice and humans suggest that heterozygosity in mastocytes is dispensable for tumour development (28). Our observations are consistent with these latter findings as NFs develop in both $Nf1^{+/-}$ and wild type backgrounds. Another difference is that all BC cell derivatives have undergone a homozygous loss of *Nf1* in our model, whereas this condition is sporadic in human. A key factor might be the difference in lifetime of both species. Only a minority of the possible

Downloaded from http://aacrjournals.org/cancerdiscovery/article-pdf/doi/10.1158/2159-8290.CD-18-0156/2929956/2159-8290_cd-18-0156v1.pdf by guest on 20 October 2022

tumours might develop during the short lifetime of the mouse, an interpretation supported by the dramatic density of tumours observed in a 20-month-old mutant animal. In addition to NFs, all NF1 patients develop a number of pigmentary lesions, including *café au lait* macules that correspond to accumulation of epidermal melanocytes. In our model, BC-derived melanocytes carry biallelic *Nf1* loss whereas all other melanocytes are either *Nf1*$^{+/-}$ or wild type (TOM-). Although *café au lait* macules do not develop in mice, due to the absence of melanocytes in the interfollicular epidermis, we observed accumulation of *Nf1*-KO melanocytes in dermal compartment starting from late embryogenesis. Moreover, we noticed marked accumulation of *Nf1*-KO and wild type pigmented melanocytes in cNFs. This is in line with the presence of pigmented cNFs in NF1 patients. In conclusion, NF1-associated dysregulation of melanocytogenesis and/or melanin synthesis is a common feature in NF1 patients and in our model.

Finally, we found that local mechanical skin injury promotes the development of cNFs, not only at the site of the injury, but also at distant sites. Wounding *Nf1*-KO skin triggers massive local proliferation of denervated *Nf1*$^{-/-}$ SCs within the first week post-surgery, suggesting the involvement of inflammation-related signals. Consistently, transcriptome profiling of wounded vs intact control and *Nf1-KO* skin led to the identification of several candidate molecules linked to inflammation that are specifically overexpressed in *Nf1*-KO skin upon injury and may play a role in this activation of SCs. Some of them have been previously reported as highly expressed in human and/or mouse neurofibromas. Soluble factors attract particular attention as they might promote development of cNFs both locally and remotely. Modulation of the activity of such factors and/or of their receptors might constitute an interesting option to impede cNF growth.

Downloaded from http://aacrjournals.org/cancerdiscovery/article-pdf/doi/10.1158/2159-8290.CD-18-0156/2929956/2159-8290_cd-18-0156v1.pdf by guest on 20 October 2022

MATERIALS AND METHODS

Animals

Mice used in this study were housed in a temperature- and humidity-controlled vivarium on a 12 h dark-light cycle with free access to food and water. The following mouse lines were used and genotyped as described in the original publications: *Nf1*$^{flox/flox}$ and *Nf1*$^{flox/-}$ (4), *Prss56*^{Cre} (6), *R26*^{tdTom} (29), *Dhh*^{Cre} (30), *Krox20*^{Cre} (31). We bred *Prss56*^{Cre}*,R26*^{tdTom} mice with the *Nf1*$^{flox/flox}$ mice to obtain the F1 generation (*Prss56*$^{Cre/+}$*,R26*$^{tdTom/+}$*,Nf1*$^{flox/+}$); we bred F1 mice with *Nf1*$^{flox/flox}$ and *Nf1*$^{+/-}$ mice to obtain *Prss56*^{Cre}*,R26*^{tdTom}*,Nf1*$^{flox/flox}$ and *Prss56*^{Cre}*,R26*^{tdTom}*,NF1*$^{flox/-}$ mutants, respectively. *Prss56*^{Cre}*,R26*^{tdTom}*,Nf1*$^{flox/+}$ animals were used as controls. For embryo analysis, we established timed pregnancies with the morning of a vaginal plug defined as E0.5. All animal manipulations were approved by a French Ethical Committee (APAFIS#1882-2015092215426712) and were performed according to French and European Union regulations.

Skin incisions and tissue processing

3-month-old control and *Nf1*-KO mice were anesthetized with Isoflurane. Dorsal skin at the lateral thoracic level was shaved and disinfected with 70% ethanol. Preoperative analgesia was applied using subcutaneous injection of Buprenorphine (0.1 mg/kg). 5 mm-long full-thickness incisions were performed unilaterally with surgical micro-scissors and sutured. Animals were perfused with 4% paraformaldehyde (PFA) on day 2, 4, 7 and 14 after surgery, and 7 months after surgery. The back skin was dissected and processed for immunohistochemical analysis. The 14 dpi wounds and unwounded skin of three *Nf1*-KO and three control animals were excised post-portem, cleaned of subcutaneous fat and homogenized in RNA lysis buffer for subsequent RNA isolation (RNesay Micro Kit, Qiagen).

Downloaded from http://aacrjournals.org/cancerdiscovery/article-pdf/doi/10.1158/2159-8290.CD-18-0156/2929956/2159-8290_cd-18-0156v1.pdf by guest on 20 October 2022

Electron microscopy

For standard ultrastructure analysis, mice were perfused with 4% PFA/1.6% glutaraldehyde (Polysciences) in 0.1 M phosphate buffer. Dorsal skin, nerve roots and subcutaneous nerves were dissected and post-fixed in the same solution overnight at 4°C, followed by embedding in Epon as previously described (6). Semi-thin sections (1 μm) were stained with toluidine blue and ultra-thin sections were stained with Uranyl Acetate and analysed using a Jeol microscope. For immuno-electron microscopy, mice were perfused with 4% PFA/0.5% glutaraldehyde and samples were embedded in LR white (Sigma Aldrich) as described (11). TOM-expressing cells were detected using rabbit anti-RFP antibody (1:20, Rockland #600-401-379).

Statistical analysis

Statistical analyses were carried out using two-tailed Student t-tests or non-parametric Mann-Whitney tests (for quantification of the melanocyte lineage and electron microscopy-based counting), and p-values considered significant are indicated by asterisks as follows: $*p < 0.05$, $**p < 0.01$, and $***p < 0.001$. Statistical analyses and scatter plots were generated using the GraphPad Prism 6.0 package. The data are represented as mean values ± standard deviation (SD) or standard error of the mean (SEM).

Analysis of cell proliferation

Pregnant mice were intraperitoneally injected with EdU at the dose of 20 mg per kg of body mass at embryonic age E18.5 and newborn pups were collected 24h later. Three *Nf1*-KO and two control littermates were decapitated, and their skin was dissected and fixed overnight in 4% PFA. EdU detection was performed on 20 μm-thick cryosections using the Click-IT Plus

Downloaded from http://aacrjournals.org/cancerdiscovery/article-pdf/doi/10.1158/2159-8290.CD-18-0156/2929956/2159-8290_cd-18-0156v1.pdf by guest on 20 October 2022

EdU Alexa Fluor 488 Imaging Kit (Thermo Fisher Scientific) according to the manufacturer's instructions, followed by immunolabelling for TOM and TRP2. Numbers of proliferating Schwann cells (TOM+/TRP2-/EdU+) were normalised against the total number of traced (TOM+/TRP2-) SCs. Quantifications were performed on 4 distant sections from each individual (~24 fields per sample) using 25X magnification under a TCS SP5 confocal microscope. The two-tailed Mann-Whitney test was used for statistical analysis. P values < 0.05 were considered statistically significant.

Library preparation, RNA sequencing and data analysis

cDNA libraries, RNA sequencing library preparation and Illumina sequencing were performed at the Ecole normale supérieure genomic core facility (Paris, France). 10 ng of total RNA was amplified and converted to cDNA using SMART-Seq v4 Ultra Low Input RNA kit (Clontech). An average of 200 pg of amplified cDNA was used for library preparation using Nextera XT DNA kit (Illumina). Libraries were multiplexed by 38 on 3 high output flow cells. 75 bp sequencing reads were performed on a NextSeq 500 device (Illumina). The analyses were performed using the Eoulsan pipeline (32), including read filtering, mapping, alignment filtering, read quantification, normalization and differential analysis. Prior to mapping, poly-N read tails were trimmed, reads ≤40 bases and with mean quality ≤30 were discarded. Reads were then aligned against the Mus Musculus genome from Ensembl version 91 using STAR (version 2.5.2) (33). Alignments from reads matching more than once on the reference genome were removed using Java version of SamTools (34). To compute gene expression, Mus musculus GFF3 genome annotation version 91 from Ensembl database was used. All overlapping regions between alignments and referenced exons were counted using HTSeq-count 0.5.3 (35). The sample counts were normalized, then statistically analyzed using DESeq 1.8.3. P-value <0.05 and FC>4x were

Downloaded from http://aacrjournals.org/cancerdiscovery/article-pdf/doi/10.1158/2159-8290.CD-18-0156/2929956/2159-8290_cd-18-0156v1.pdf by guest on 20 October 2022

used as cutoffs criteria to select differentially expressed genes (DEGs). The RNA-seq gene expression data and raw Fastq files are available on the GEO repository (www.ncbi.nlm.nih.gov/geo/) under accession number GSE117781.

Pathway over-representation analysis was performed using the WebGestalt web server (http://www.webgestalt.org). DEG sets were queried against the KEGG database using FDR q<0.05 cutoff to select significantly enriched pathways.

Downloaded from http://aacrjournals.org/cancerdiscovery/article-pdf/doi/10.1158/2159-8290.CD-18-0156/2929956/2159-8290_cd-18-0156v1.pdf by guest on 20 October 2022

ACKNOWLEGMENTS

The P.C. laboratory was financed by the Institut National de la Recherche Médicale (INSERM), the Centre National de la Recherche Scientifique (CNRS), the Ministère de la Recherche et Technologie (MRT), the Fondation pour la Recherche Médicale (FRM), and the Association de Recherche sur le Cancer (ARC). It has received support under the program “Investissements d’Avenir” launched by the French Government and implemented by the ANR, with the references: ANR-10-LABX-54 MEMOLIFE and ANR-11-IDEX-0001-02 PSL* Research University. KJR was financed by ARC, n°PDF20150603033. PT received financial support for this study from the Neurofibromatosis Therapeutic Acceleration Program (NTAP). The NTAP is a philanthropy-driven research program based at the Johns Hopkins University School of Medicine. This work was supported in part by Bloomberg Philanthropies (www.bloomberg.org). Its contents are solely the responsibilities of the authors and do not necessarily represent the official views of Bloomberg Philanthropies or The Johns Hopkins University. We are grateful to the IBENS Imaging Facility, which received the support of grants from the “Région Ile-de-France” (NERF N°2011-45), the “Fondation pour la Recherche Médicale” (N° DGE 20111123023) and the “Fédération pour la Recherche sur le Cerveau - Rotary International France” (2011). The IBENS Imaging Facility has also received support implemented by the ANR under the program «Investissements d’Avenir», with the references: ANR-10-LABX-54 MEMO LIFE, ANR-11-IDEX-0001-02 PSL* Research University and ANR-10-INSB-04-01 France-BioImaging infrastructure. The IBENS Genomic Facility was supported by the France Génomique national infrastructure, funded as part of the "Investissements d'Avenir" program managed by the Agence Nationale de la Recherche (contract ANR-10-INBS-09). We thank Graziella Matesic, Laurence Richard and

Downloaded from http://aacrjournals.org/cancerdiscovery/article-pdf/doi/10.1158/2159-8290.CD-18-0156/2929956/2159-8290_cd-18-0156v1.pdf by guest on 20 October 2022

Carole Kesrouani for technical assistance and Victor Riccardi for critical reading of the manuscript.

Downloaded from http://aacrjournals.org/cancerdiscovery/article-pdf/doi/10.1158/2159-8290.CD-18-0156/2929956/2159-8290_cd-18-0156v1.pdf by guest on 20 October 2022

REFERENCES

1. Ratner N, Miller SJ. A RASopathy gene commonly mutated in cancer: the neurofibromatosis type 1 tumour suppressor. Nat Rev Cancer. 2015;15:290–301.

2. Parrinello S, Lloyd AC. Neurofibroma development in NF1--insights into tumour initiation. Trends in Cell Biology. 2009;19:395–403.

3. Maro GS, Vermeren M, Voiculescu O, Melton L, Cohen J, Charnay P, et al. Neural crest boundary cap cells constitute a source of neuronal and glial cells of the PNS. Nature Neuroscience. 2004;7:930–8.

4. Zhu Y, Ghosh P, Charnay P, Burns DK, Parada LF. Neurofibromas in NF1: Schwann cell origin and role of tumor environment. Science. 2002;296:920–2.

5. Coulpier F, Le Crom S, Maro GS, Manent J, Giovannini M, Maciorowski Z, et al. Novel features of boundary cap cells revealed by the analysis of newly identified molecular markers. Glia. 2009;57:1450–7.

6. Gresset A, Coulpier F, Gerschenfeld G, Jourdon A, Matesic G, Richard L, et al. Boundary Caps Give Rise to Neurogenic Stem Cells and Terminal Glia in the Skin. Stem Cell Reports. 2015;5:278–90.

7. Joseph NM. Neural crest stem cells undergo multilineage differentiation in developing peripheral nerves to generate endoneurial fibroblasts in addition to Schwann cells. Development. 2004;131:5599–612.

8. Richard L, Topilko P, Magy L, Decouvelaere A-V, Charnay P, Funalot B, et al. Endoneurial fibroblast-like cells. J Neuropathol Exp Neurol. 2012;71:938–47.

9. Cauna N. The free penicillate nerve endings of the human hairy skin. J Anat. 1973;115:277–88.

10. Reinisch CM, Tschachler E. The dimensions and characteristics of the subepidermal nerve plexus in human skin – Terminal Schwann cells constitute a substantial cell population within the superficial dermis. Journal of Dermatological Science. 2012;65:162–9.

11. Peltonen J, Jouhilahti E-M, Peltonen S. Molecular and Cellular Basis of Human Cutaneous Neurofibromas and Their Development. Neurofibromatosis Type 1. Berlin, Heidelberg: Springer, Berlin, Heidelberg; 2012. pages 393–403.

12. Stemmer-Rachamimov AO, Louis DN, Nielsen GP, Antonescu CR, Borowsky AD, Bronson RT, et al. Comparative pathology of nerve sheath tumors in mouse models and humans. Cancer Res. American Association for Cancer Research; 2004;64:3718–24.

13. Basbaum AI, Bautista DM, Scherrer G, Julius D. Cellular and molecular mechanisms of pain. Cell. 2009;139:267–84.

Downloaded from http://aacrjournals.org/cancerdiscovery/article-pdf/doi/10.1158/2159-8290.CD-18-0156/2929956/2159-8290_cd-18-0156v1.pdf by guest on 20 October 2022

14. Riccardi VM. Cutaneous manifestation of neurofibromatosis: cellular interaction, pigmentation, and mast cells. Birth Defects Orig Artic Ser. 1981;17:129–45.

15. Singer AJ, Clark RA. Cutaneous wound healing. N Engl J Med. 1999 Sep 2;341(10):738–46.

16. Parfejevs V, Debbache J, Shakhova O, Schaefer SM, Glausch M, Wegner M, et al. Injury-activated glial cells promote wound healing of the adult skin in mice. Nat Comms. Springer US; 2017;:1–16.

17. Eming SA, Martin P, Tomic-Canic M. Wound repair and regeneration: Mechanisms, signaling, and translation. Science Translational Medicine. 2014;6:265sr6–265sr6.

18. Choi K, Komurov K, Fletcher JS, Jousma E, Cancelas JA, Wu J, et al. An inflammatory gene signature distinguishes neurofibroma Schwann cells and macrophages from cells in the normal peripheral nervous system. Nature Publishing Group. Nature Publishing Group; 2017;:1–14.

19. Karaosmanoglu B, Kocaefe ÇY, Söylemezoğlu F, Anlar B, Varan A, Vargel İ, et al. Heightened CXCR4 and CXCL12 expression in NF1-associated neurofibromas. Child's Nervous System; 2018;:1–6.

20. Ishida Y, Gao JL, Murphy PM. Chemokine Receptor CX3CR1 Mediates Skin Wound Healing by Promoting Macrophage and Fibroblast Accumulation and Function. The Journal of Immunology. 2007;180:569–79.

21. Pong WW, Higer SB, Gianino SM, Emnett RJ, Gutmann DH. Reduced microglial CX3CR1 expression delays neurofibromatosis-1 glioma formation. Ann Neurol. Wiley-Blackwell; 2013;73:303–8.

22. Wu J, Williams JP, Rizvi TA, Kordich JJ, Witte D, Meijer D, et al. Plexiform and dermal neurofibromas and pigmentation are caused by Nf1 loss in desert hedgehog-expressing cells. Cancer Cell. 2008;13:105–16.

23. Topilko P, Schneider-Maunoury S, Levi G, Baron-Van Evercooren A, Chennoufi AB, Seitanidou T, et al. Krox-20 controls myelination in the peripheral nervous system. Nature. 1994;371:796–9.

24. Gambardella L, Schneider-Maunoury S, Voiculescu O, CHARNAY P, Barrandon Y. Pattern of expression of the transcription factor Krox-20 in mouse hair follicle. Mechanisms of Development. 2000;96:215–8.

25. Drouet A, Wolkenstein P, Lefaucheur J-P, Pinson S, Combemale P, Gherardi RK, et al. Neurofibromatosis 1-associated neuropathies: a reappraisal. Brain. 2004;127:1993–2009.

26. Jouhilahti E-M, Peltonen S, Callens T, Jokinen E, Heape AM, Messiaen L, et al. The Development of Cutaneous Neurofibromas. The American Journal of Pathology. American Society for Investigative Pathology; 2011;178:500–5.

Downloaded from http://aacrjournals.org/cancerdiscovery/article-pdf/doi/10.1158/2159-8290.CD-18-0156/2929956/2159-8290_cd-18-0156v1.pdf by guest on 20 October 2022

27. Yang F-C, Ingram DA, Chen S, Zhu Y, Yuan J, Li X, et al. Nf1-Dependent Tumors Require a Microenvironment Containing Nf1+/−- and c-kit-Dependent Bone Marrow. Cell. 2008;135:437–48.

28. Liao C-P, C Booker R, Brosseau J-P, Chen Z, Mo J, Tchegnon E, et al. Contributions of inflammation and tumor microenvironment to neurofibroma tumorigenesis. Journal of Clinical Investigation. 2018;:1–42.

29. Madisen L, Zwingman TA, Sunkin SM, Oh SW, Zariwala HA, Gu H, et al. A robust and high-throughput Cre reporting and characterization system for the whole mouse brain. Nature Neuroscience. Nature Publishing Group; 2009;13:133–40.

30. Jaegle M, Ghazvini M, Mandemakers W, Piirsoo M, Driegen S, Levavasseur F, et al. The POU proteins Brn-2 and Oct-6 share important functions in Schwann cell development. Genes & Development. 2003;17:1380–91.

31. Voiculescu O, Charnay P, Schneider-Maunoury S. Expression pattern of aKrox-20/Cre knock-in allele in the developing hindbrain, bones, and peripheral nervous system. genesis. 2000;26:123–6.

32. Jourdren L, Bernard M, Dillies M-A, Le Crom S. Eoulsan: a cloud computing-based framework facilitating high throughput sequencing analyses. Bioinformatics. 2012;28:1542–3.

33. Dobin A, Davis CA, Schlesinger F, Drenkow J, Zaleski C, Jha S, et al. STAR: ultrafast universal RNA-seq aligner. Bioinformatics. 2012;29:15–21.

34. Li H, Handsaker B, Wysoker A, Fennell T, Ruan J, Homer N, et al. The Sequence Alignment/Map format and SAMtools. Bioinformatics. 2009;25:2078–9.

35. Anders S, Pyl PT, Huber W. HTSeq--a Python framework to work with high-throughput sequencing data. Bioinformatics. 2015;31:166–9.

Downloaded from http://aacrjournals.org/cancerdiscovery/article-pdf/doi/10.1158/2159-8290.CD-18-0156/2929956/2159-8290_cd-18-0156v1.pdf by guest on 20 October 2022

FIGURE LEGENDS

Figure 1: Tracing of Prss56-positive BC cell derivatives in the adult PNS

(A-D) Analysis of BC cell derivatives (TOM+) in the adult nerve roots of *Prss56*^{Cre}, *R26*^{tdTom} mice. (A) Transverse section through the cervical spinal cord reveals the presence of numerous TOM+ cells along the dorsal and ventral nerve roots and in the DRG. Inset shows a transverse section through the dorsal root. (B-D) Most nerve root TOM+ cells express S100 (B, D) and SOX10 (C) and correspond to SCs (full arrowheads in B and D). Note the presence TOM+/S100- endoneurial cells (open arrowheads in B) and TOM- perineurial fibroblasts (see also Fig. S1C). Spc, spinal cord; DR, dorsal root; VR, ventral root; DRG, dorsal root ganglion; Nu, nuclear labelling. (E-K') Analysis of BC cell derivatives in the dorsal skin of adult *Prss56*^{Cre}, *R26*^{tdTom} mice. (E, F) Dorsal (epidermal) and ventral (hypodermal) views of the back skin showing direct TOM fluorescence. Note the patch-like distribution of TOM+ cells. (G) Transverse section of the skin immunolabelled with TOM and a SC marker S100. TOM+ cells are associated with dermal and hypodermal innervation (arrowheads in G and arrow in F, respectively) and correspond to nmSCs, including lanceolate glia (G, H), arrector pili glia (G, I) and subepidermal glia (G, J). (I and J) are dorsal views of whole-mount skin co-labelled with TOM and axonal marker TUJ1. (K, K') TOM+ pigmented melanocytes within a hair follicle. TOM staining merged with a bright field image (K') reveals melanin granules (dark pigment). Epi, epidermis; der, dermis; hyp, hypodermis; HF, hair follicle. Scale bar: 50 µm (A-D, G-K'), 1 mm (E, F).

Figure 2: Targeted *Nf1* inactivation in the BC cell lineage gives rise to paraspinal and subcutaneous plexiform NFs

Downloaded from http://aacrjournals.org/cancerdiscovery/article-pdf/doi/10.1158/2159-8290.CD-18-0156/2929956/2159-8290_cd-18-0156v1.pdf by guest on 20 October 2022

(A) Global view of control (left) and *Nf1*-KO mutant (right) spinal cords with attached nerve roots from 11-month-old animals. Paraspinal tumours are present in the mutant at the cervical and thoracic levels (arrowheads). (B, C) Higher magnifications of the control (B) and *Nf1*-KO mutant (C) thoracic regions showing enlargement of the mutant nerve roots (full arrowheads) and adjacent DRGs (empty arrowheads) caused by accumulation of TOM+ cells. (D) Section though this region showing compression of the spinal cord by the TOM+/S100+ tumour mass. (E-G'') Increasing magnifications through a neurofibroma immunolabelled for TOM, S100 and TUJ1. Strongly S100+ mSCs (always in contact with large-calibre axons) are intermixed with randomly organised TOM+ cells that are weakly S100+ (full arrowheads in G-G'') or S100- (empty arrowheads in G-G''). Ultrastructure analysis of control (H) and *Nf1*-KO (I-K) nerve roots revealed an enlargement of the extracellular compartment and disruption of Remak bundles (arrowhead) in the mutant. Normal Remak SCs are shown in H (arrowhead and inset). Mutant nmSCs ensheath fewer axons or are devoid of axonal contact and extend slender protrusions that enwrap collagen fibrils (J) or myelinated fibres (K). nmSCs are pseudocoloured in red in (H, J and K). (L) Subcutaneous nerve showing the local enlargement corresponding to a subcutaneous plexiform NF (spNF, arrowhead). (M-O) Sections through an spNF immunolabelled for TOM, S100 and PDGFRα (fibroblasts) reveal expansion of traced SCs and non-traced fibroblasts. (N-O) correspond to the boxed area in (M). (P) Electron microscopy micrograph of the spNF shows disrupted Remak bundles (arrows) and abnormal perineurial sheath (arrowheads). Spc, spinal cord; DR, dorsal root; DRG, dorsal root ganglion; m, myelinating Schwann cell: a, axons. Scale bar: 1 mm (A-C, L), 50 µm (D-F, M-O), 1µm (H-K, P).

Figure 3: Mice with *Nf1* loss-of-function in BC cell derivatives develop diffuse cutaneous NFs

Downloaded from http://aacrjournals.org/cancerdiscovery/article-pdf/doi/10.1158/2159-8290.CD-18-0156/2929956/2159-8290_cd-18-0156v1.pdf by guest on 20 October 2022

(A) 19-month-old *Nf1*-KO mutant showing pruritic skin lesions (arrows) at cervical and thoracic levels. (B) Numerous small lesions present on the back skin (arrowheads) showing direct TOM fluorescence (inset). (C-G') Immunohistochemical analysis of cNF reveals accumulations of TOM+/S100+ SCs with aberrant morphologies (C, D'), and heavy infiltration of KIT+ mastocytes (E, E'), IBA1+ macrophages (F, F') and PDGFRα+ fibroblasts (G, G'). Control skin is shown on the bottom left of each figure. Insets in (E-G) represent low magnifications of the corresponding images with TOM labelling. Dotted lines indicate the upper tissue limits and the boundaries between dermis and hypodermis. KIT staining within hair follicles (HF) in (C') corresponds to melanocytes. (H) Dense collagen accumulation in cNF revealed by sirius red staining (red). (I) Extrafollicular pigmentation in cNF. Inset shows higher magnification of TOM+ and TOM- pigmented cells (dark granules). Dotted lines encircle hair follicles containing pigmented hair shafts. (J, K) Electron microscopy micrographs showing SC cytoplasmic protrusions (arrowheads in J) unsheathing isolated axons (a) and/or collagen fibrils (inset in J). (K) Immunoelectron micrograph of mutant SC (pseudocoloured in red) without axonal contact at the level of the soma. Dark granules correspond to TOM staining. Scale bar: 5 mm (B); 100 µm (C-I), 1 µm (J, K).

Figure 4: *Nf1* loss-of-function in BC cells promotes proliferation of dermal Schwann cell and melanocyte lineages

(A-J) Comparison of control and *Nf1*-KO newborn skin immunolabeled for TOM, TUJ1 (nerves) and TRP2 (melanocytes) (A, B, D, E), and PDGFRα (fibroblasts; H and I) show expansion of traced BC derivatives, including SCs (nerve associated TOM+/TRP2- cells; D and E arrows) and melanocytes (nerve-free TOM+/TRP2+ cells; D and E arrowheads), but not of dermal fibroblasts in the mutant dermis. Insets in (D and E) show higher magnifications of the indicated area. (C, F, G, J) Quantification of traced SCs (C), traced follicular and

Downloaded from http://aacrjournals.org/cancerdiscovery/article-pdf/doi/10.1158/2159-8290.CD-18-0156/2929956/2159-8290_cd-18-0156v1.pdf by guest on 20 October 2022

extrafollicular melanocytes (F), non-traced KIT+ mastocytes (G) and IBA1+ macrophages (J) in control vs *Nf1*-KO P0 skin. (K-O'') Comparison of 3-months-old control and *Nf1*-KO mutant skin immunolabeled for TOM and TUJ1 (K and L) reveals further expansion and morphological abnormalities of the traced SC population in the mutant. (M) Quantification of traced SCs in the control and *Nf1*-KO dermis. (N, O) Dorsal views of clarified skin at the level of subepidermal nerve plexus. (O', O'') show higher magnifications of mutant subepidermal SCs. Note numerous cytoplasmic extensions (arrowheads) and a SC soma (arrow) detached from the adjacent axon bundle. Asterisks indicate SC somas. (P, Q) Staining of PDGFRα+ dermal fibroblasts reveal a dramatic expansion of this population in the mutant dermis. (R) Quantification of non-traced KIT+ mastocytes in the control and *Nf1*-KO dermis. Data are represented as mean values ± SD. Each data point corresponds to a number of cells per field of view. Fold change (FC) differences are given for each comparison. Scale bar: 50 μm.

Figure 5: 6-month-old *Nf1*-KO mutant skin contains numerous micro-cNFs

(A, B) Transverse sections through *Nf1*-KO mutant (A) and control (B) skin reveal local accumulations of TOM+ cells in the mutant dermis. The dotted lines indicate upper tissue limits and the boundaries between the dermis (der) and the hypodermis (hyp). (C) High magnification view of the mutant dermis shows abnormal morphology of TOM+/S100+ SCs. (D) Quantification of the relative abundance of different cell types in micro-cNFs and control skin. The data are represented as mean values measured per 0.026 μm^2 ± SEM (*** $p<0.0001$). Fold change differences are given for each comparison. SC unit refers to SC soma or fragment of SC cytoplasm (> 2 μm). (E, F) Electron micrographs showing typical non-myelinated nerve fibres in the control dermis (E) and a disrupted Remak bundle in a micro-cNF (F). Arrow indicates the perikaryon of a mutant SC devoid of axonal contact, and

Downloaded from http://aacrjournals.org/cancerdiscovery/article-pdf/doi/10.1158/2159-8290.CD-18-0156/2929956/2159-8290_cd-18-0156v1.pdf by guest on 20 October 2022

arrowheads indicate abnormal cytoplasmic extensions, often enwrapping pairs or single axons separated by collagenous extracellular matrix. a, axon; Nu, cell nucleus. (G-H’) Global (G, H) and higher magnification (G’, H’) views of the mutant skin in the upper and lower dermis showing aggregates of TOM+ SCs with abnormal morphologies. Most SCs extend abnormal cytoplasmic protrusions (arrowheads) or appear to be detached from the axons (arrows). Scale bar: 50 µm (A-C, G-H’), 1 µm (E, F).

Downloaded from http://aacrjournals.org/cancerdiscovery/article-pdf/doi/10.1158/2159-8290.CD-18-0156/2929956/2159-8290_cd-18-0156v1.pdf by guest on 20 October 2022

Figure 6: Skin injury promotes development of cNFs in *Nf1*-KO mice

(Panel A) Comparison of *Nf1*-KO and control skin at 7 months post-injury. (a) Dorsal skin from a 10-month-old injured *Nf1*-KO mutant with multiple discrete skin (pale spots) and crusty lesions (arrowheads) all over the back skin. (b, c) Distribution of TOM+ cells in the thoracic skin of 10-month-old *Nf1*-KO mutant (b), and control (c) injured mice (dotted line indicates the site of incision). (d-e’) Lumbar skin from a 10-month-old injured *Nf1*-KO mouse (d, d’) and an age-matched uninjured *Nf1*-KO mutant (e, e’). Note in (d) the presence of numerous pale spots (arrowheads). (d’, e’) Higher magnification of the lumbar skin with direct TOM fluorescence. Arrowheads indicate aggregates of TOM+ cells, related to pale spots in (d). (f-h) Transverse sections through thoracic (f) and lumbar (g) skin from the injured *Nf1*-KO animal and lumbar skin from the uninjured mutant (h). Dense accumulations of TOM+ cells are observed in the dermis, both at sites close to (f) and distant from (g, arrowheads) the injury. The skin from uninjured *Nf1*-KO contains only microscopic lesions, corresponding to micro-cNFs (arrowhead in h and magnified view in the inset). (i-k) Injury site shows a cell composition typical of cNFs, with accumulation of TOM+/S100+ SCs with aberrant morphologies (i), KIT+ mastocytes, IBA1+ macrophages (j) and PDGFRα+ fibroblasts (k). Dotted line in f-h: boundary between dermis and hypodermis. (Panel B) Time course analysis of wounded control (CTRL) and *Nf1*-KO skin. (a-h) Tracing of wild type (a, c, e, g) and *Nf1*-KO (b, d, f, h) TOM+ SCs at 2, 4, 7 and 14 day post-injury (dpi). The arrowheads indicate the injury site. Inset in (f) shows co-expression of TOM and proliferation marker PH3. Nu; nuclear staining. (g', h') High magnification images of (g) and (h) showing TOM and axonal (TUJ1) staining. (i-p) Immunolabeling of control (i, j, m, n) and *Nf1*-KO (k, l, o, p) wound sites for S100 (SCs) (i, k), PDGFRα (fibroblasts) (j, l), IBA1 (macrophages) (m, o), and KIT (mastocytes) (n, p). Scale bar: 5 mm (A-b, c, d', e'), 500 μm (A-f-h), 50 μm (A-i-k), 100 μm (B). (Panel C) Differentially expressed genes between injured and uninjured skin and pathway enrichment analysis. (a) Significantly upregulated and downregulated genes ($p<0.05$ and FC>4) between injured (14 dpi) and uninjured skin in control and *Nf1*-KO animals. (b, c) Top-ranked enriched KEGG pathways among the upregulated genes in injured vs uninjured comparisons in *Nf1*-KO (b) and control (c) skin.

Figure 7: Tracing of the derivatives of Krox20+ and Dhh+ cells in the adult skin

(A-B'') Transverse sections of $Krox20^{Cre}$,$R26^{tdTom}$ skin stained with TOM and glial markers (A, A') and vascular markers, PECAM (endothelial cells, B-B'') and NG2 (pericytes, B'). All traced S100+ SCs are MBP+ and therefore correspond to mSCs (arrowheads in A, A'). Note that S100+/MBP- nmSCs, including Remak SCs, lanceolate and subepidermal glia, are not traced (arrows in A, A'). TOM+ cells are also present in the epidermis (keratinocytes, arrow in B), inside the hair follicle (HF) and along capillaries (arrowheads in B). (C-G') Transverse sections of Dhh^{Cre},$R26^{tdTom}$ skin stained for TOM, S100 (C-F), MBP (C), K15 (keratinocytes) and TUJ1 (axons) (G, G'). TOM+ cells correspond to a subset of mSCs (C, full arrowheads), Remak SCs (D, full arrowhead), arrector pili glia (E, arrowhead) together with arrector pili muscle (D, open arrowhead) and other muscle fibres (C, open arrowhead), lanceolate glia (F, arrowheads), and Merkel cells of the touch dome (G, arrowhead). No subepidermal glia are traced (D, arrows). (G') A higher magnification of the area indicated in (G). (H-I) Dorsal

Downloaded from http://aacrjournals.org/cancerdiscovery/article-pdf/doi/10.1158/2159-8290.CD-18-0156/2929956/2159-8290_cd-18-0156v1.pdf by guest on 20 October 2022

view of the subepidermal region from *Prss56*^{Cre}*,R26*^{tdTom} (H) and *Dhh*^{Cre}*,R26*^{tdTom} (I) adult skin. Note numerous TOM+ SCs associated with the subepidermal neuronal plexus (TUJ1-positive) in *Prss56*^{Cre}*,R26*^{tdTom} dermis and absence of TOM labelling at this level with the *Dhh*^{Cre} driver (arrowheads point to cell bodies of subepidermal SCs, empty arrowhead indicate traced Merkel cells). (J) Table summarising the type of derivatives in the adult skin traced with the three Cre drivers. Scale bar: 50 µm.

Downloaded from http://aacrjournals.org/cancerdiscovery/article-pdf/doi/10.1158/2159-8290.CD-18-0156/2929956/2159-8290_cd-18-0156v1.pdf by guest on 20 October 2022

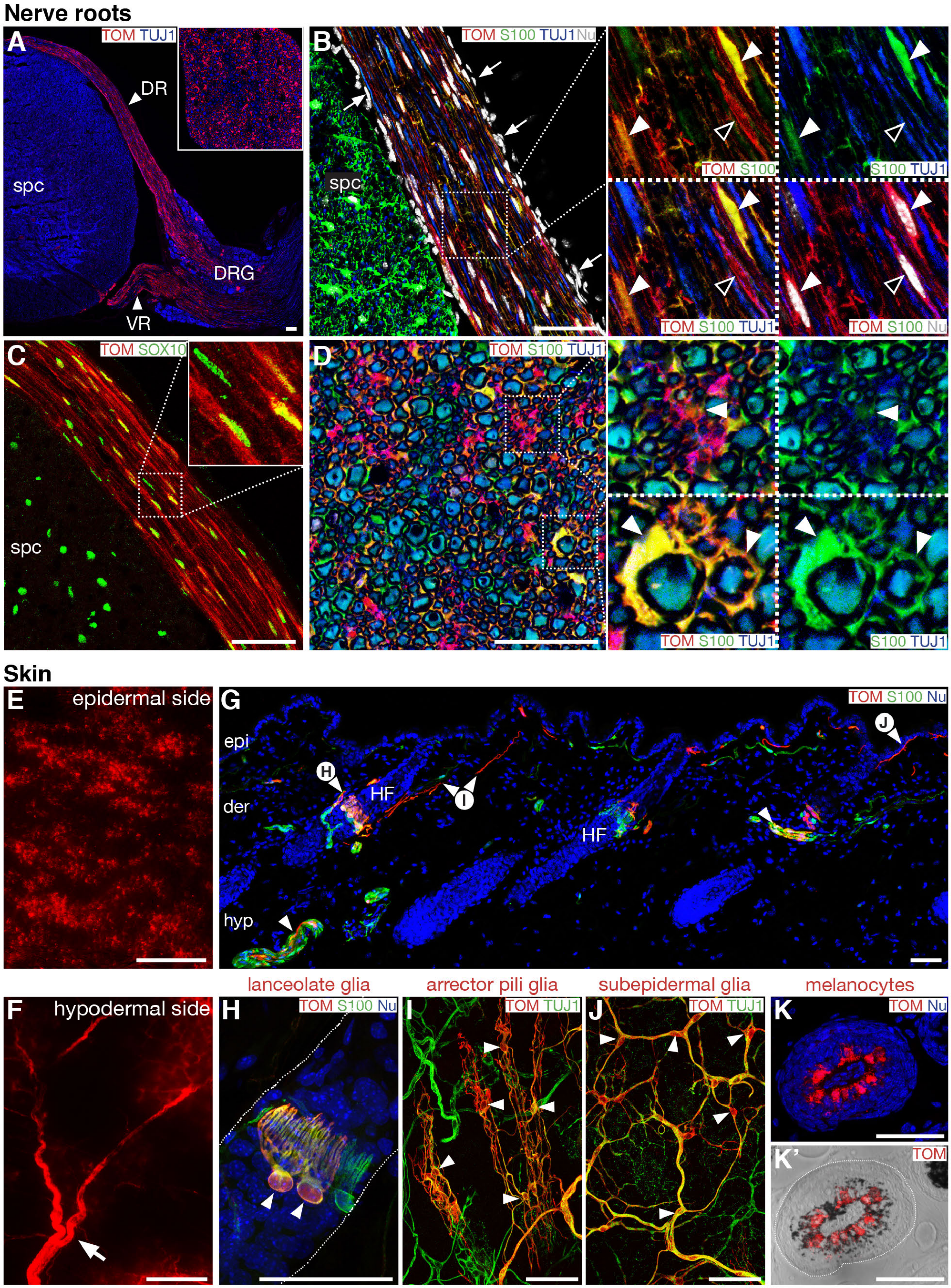

Figure 1

Downloaded from http://aacrjournals.org/cancerdiscovery/article-pdf/doi/10.1158/2159-8290.CD-18-0156/2929956/2159-8290_cd-18-0156v1.pdf by guest on 20 October 2022

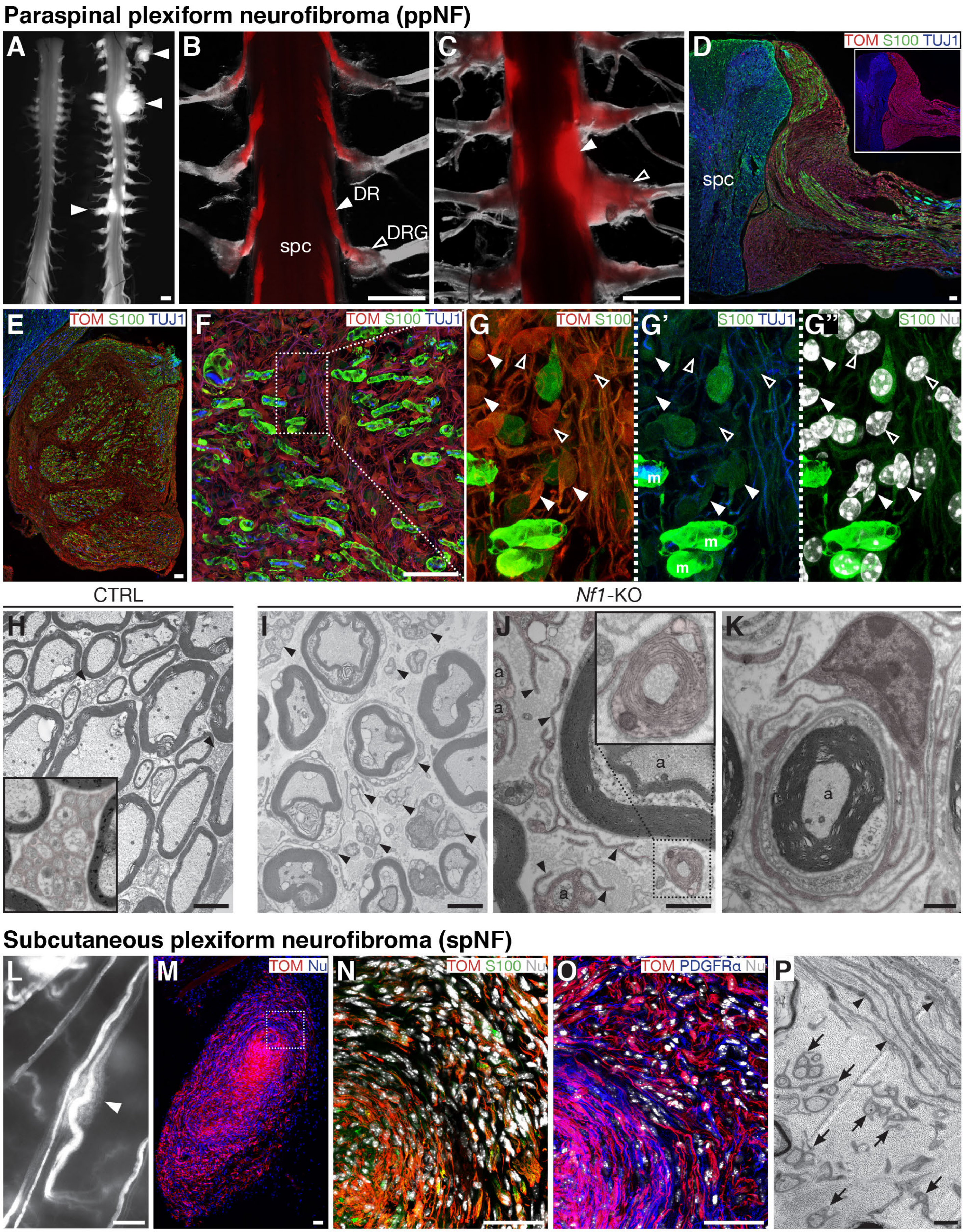

Figure 2

Downloaded from http://aacrjournals.org/cancerdiscovery/article-pdf/doi/10.1158/2159-8290.CD-18-0156/2929956/2159-8290_cd-18-0156v1.pdf by guest on 20 October 2022

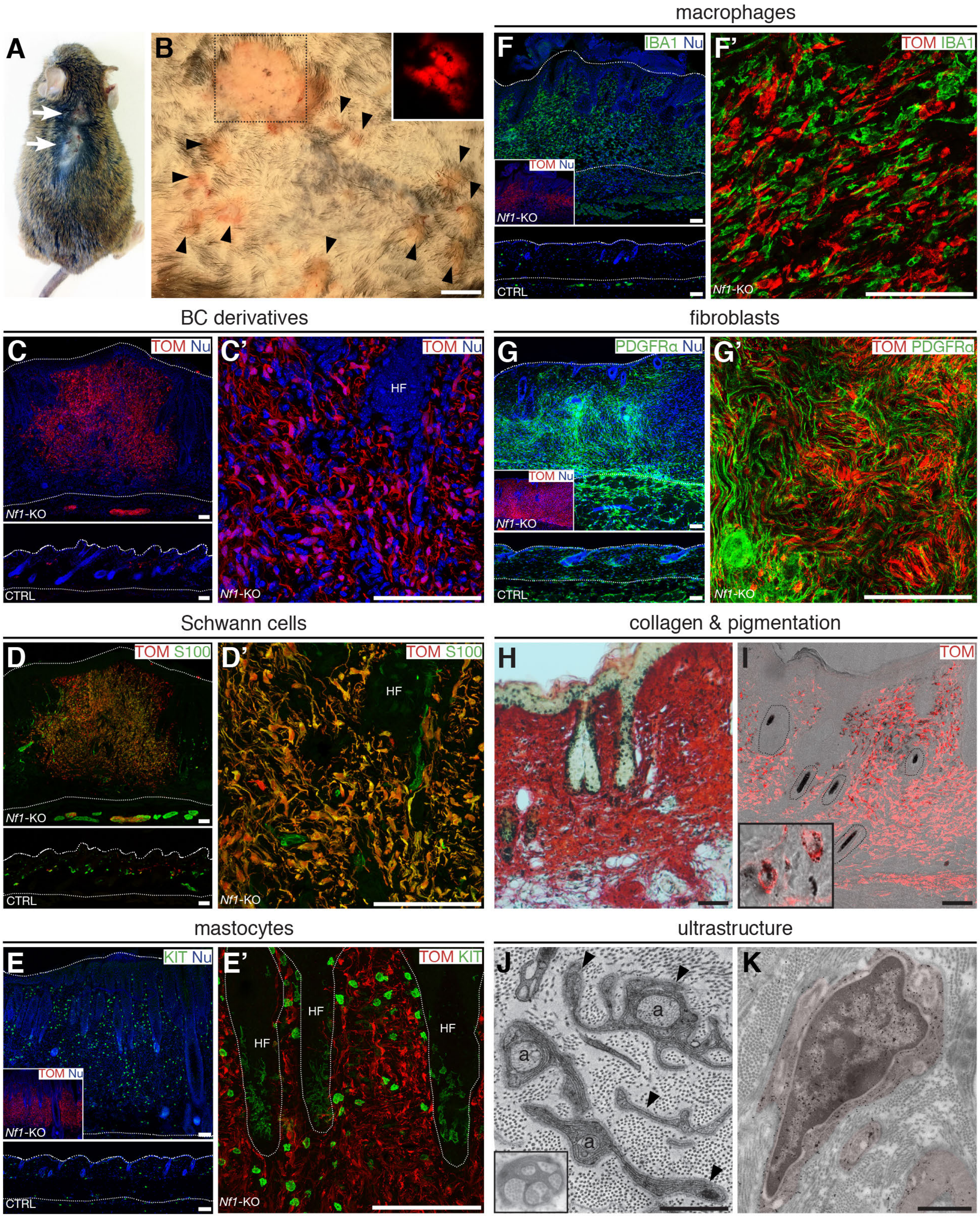

Figure 3

Downloaded from http://aacrjournals.org/cancerdiscovery/article-pdf/doi/10.1158/2159-8290.CD-18-0156/2929956/2159-8290_cd-18-0156v1.pdf by guest on 20 October 2022

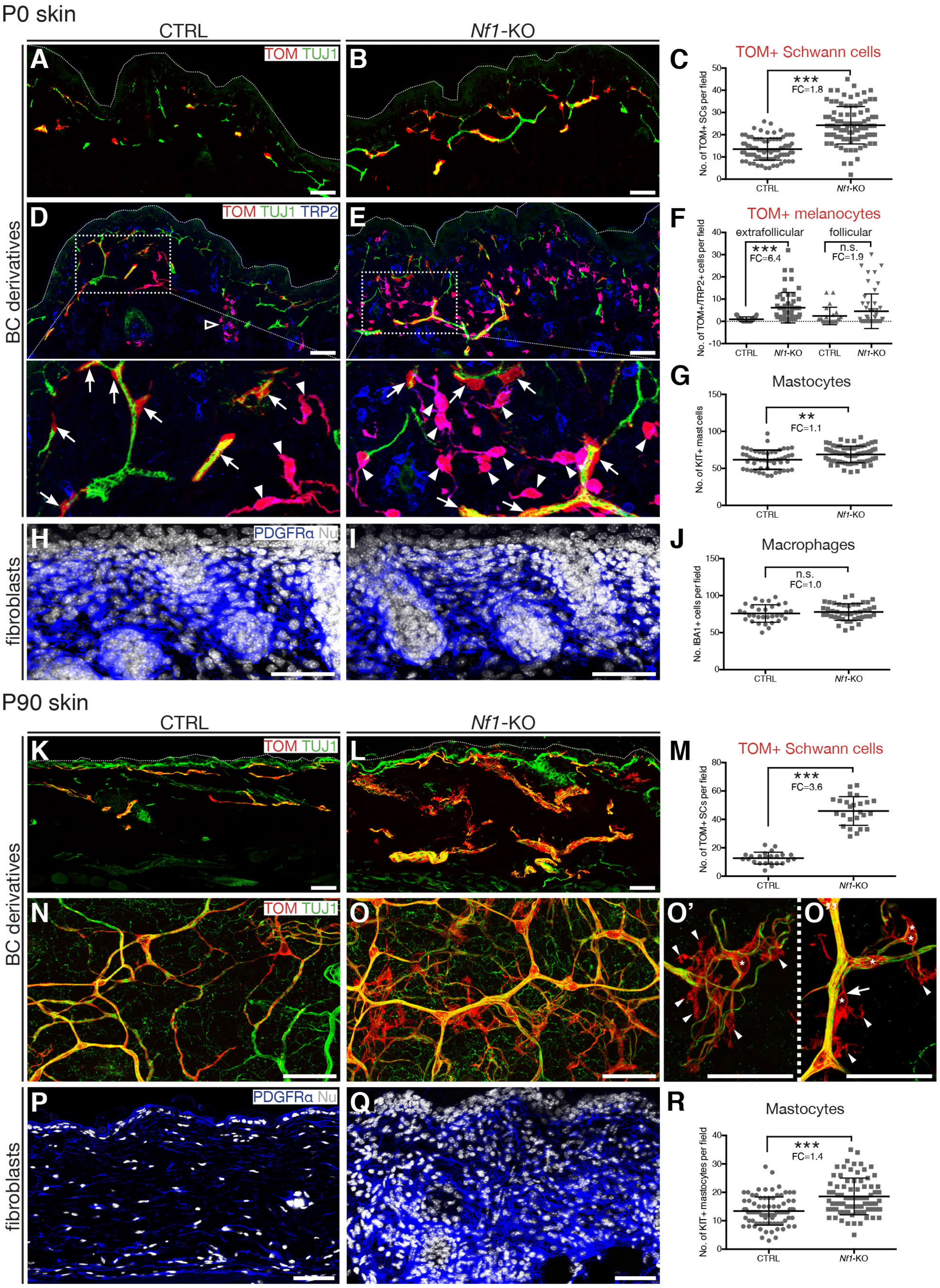

Figure 4

Downloaded from http://aacrjournals.org/cancerdiscovery/article-pdf/doi/10.1158/2159-8290.CD-18-0156/2929956/2159-8290_cd-18-0156v1.pdf by guest on 20 October 2022

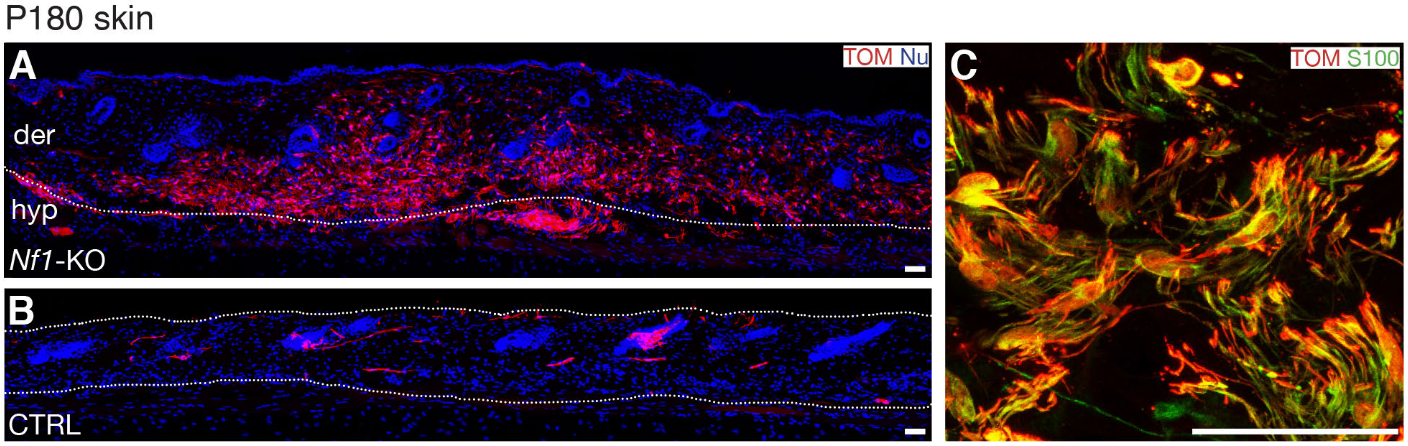

D

Cell type	CTRL	*Nf1*-KO	p value	fold change
SC units	1.52 ± 0.29	33.31 ± 3.32	***	21.9
axons	4.85 ± 0.88	10.60 ± 0.90	***	2.2
mastocytes	0.21 ± 0.06	1.83 ± 0.21	***	8.8
macrophages	0.17 ± 0.06	2.11 ± 0.34	***	12.7
fibroblasts	4.44 ± 0.30	23.09 ± 2.02	***	5.2
neutrophils	0.23 ± 0.07	9.29 ± 1.39	***	40.5
blood vessels	1.04 ± 0.49	2.19 ± 0.28	***	2.1

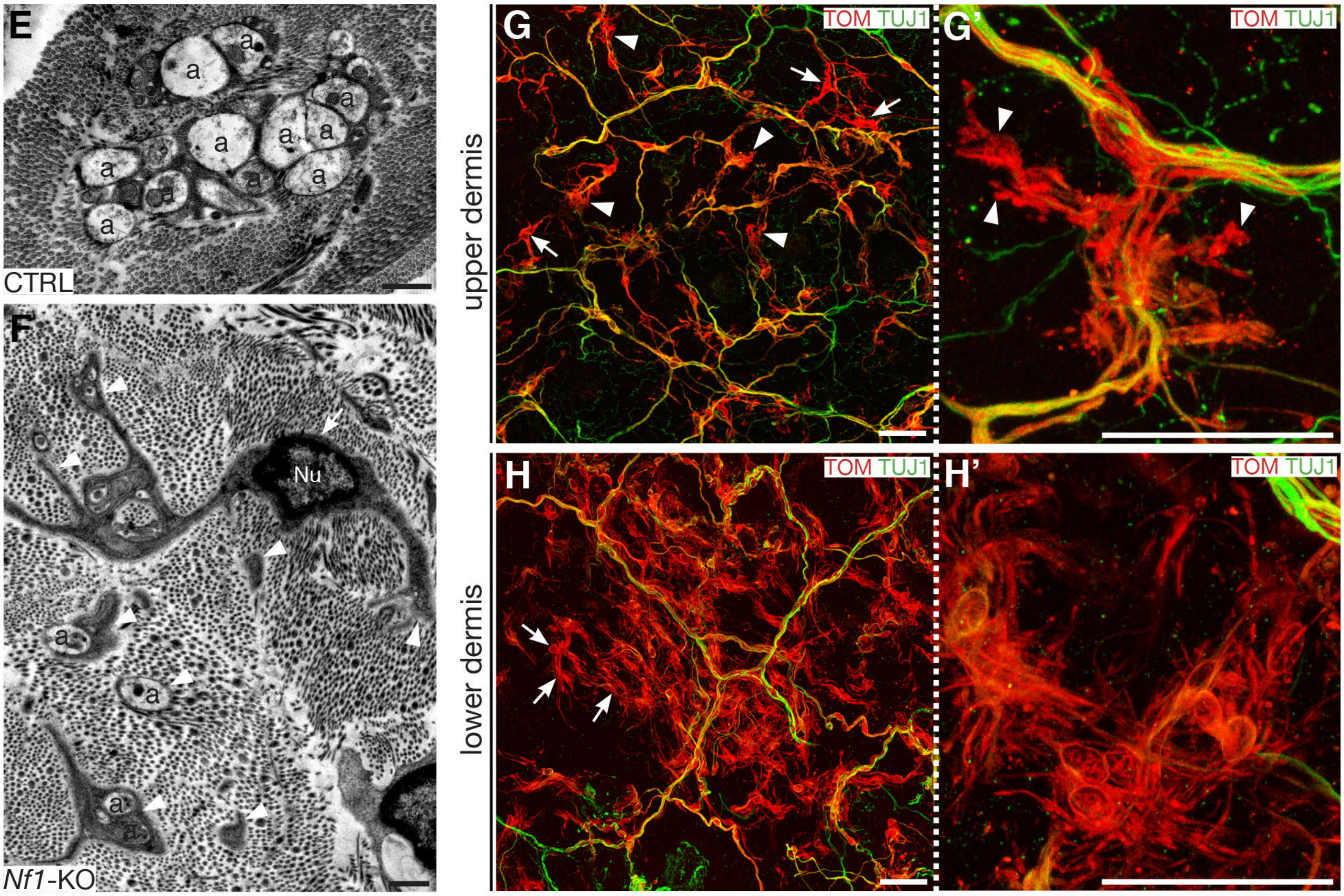

Figure 5

Downloaded from http://aacrjournals.org/cancerdiscovery/article-pdf/doi/10.1158/2159-8290.CD-18-0156/2929956/2159-8290_cd-18-0156v1.pdf by guest on 20 October 2022

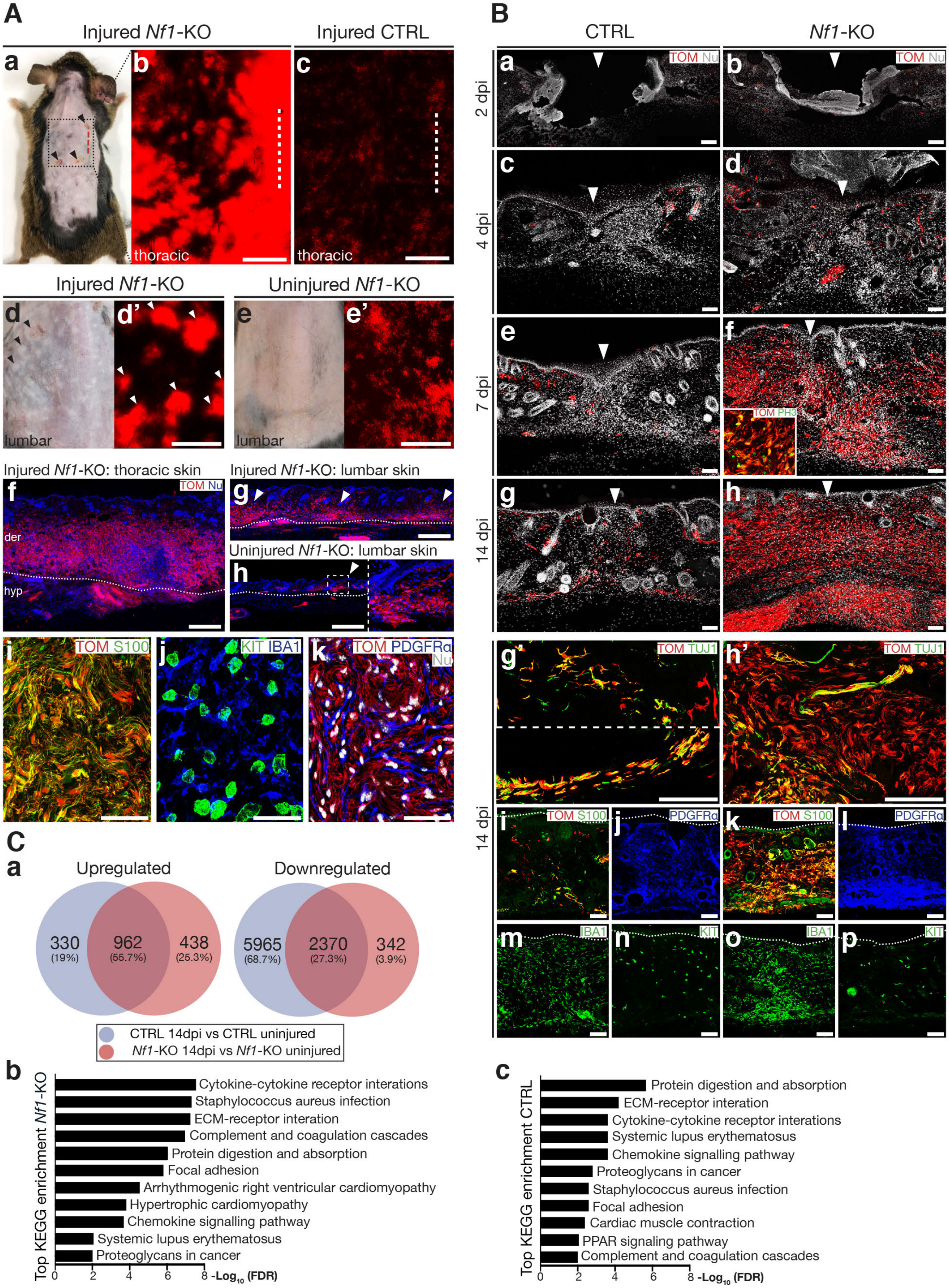

Figure 6

Downloaded from http://aacrjournals.org/cancerdiscovery/article-pdf/doi/10.1158/2159-8290.CD-18-0156/2929956/2159-8290_cd-18-0156v1.pdf by guest on 20 October 2022

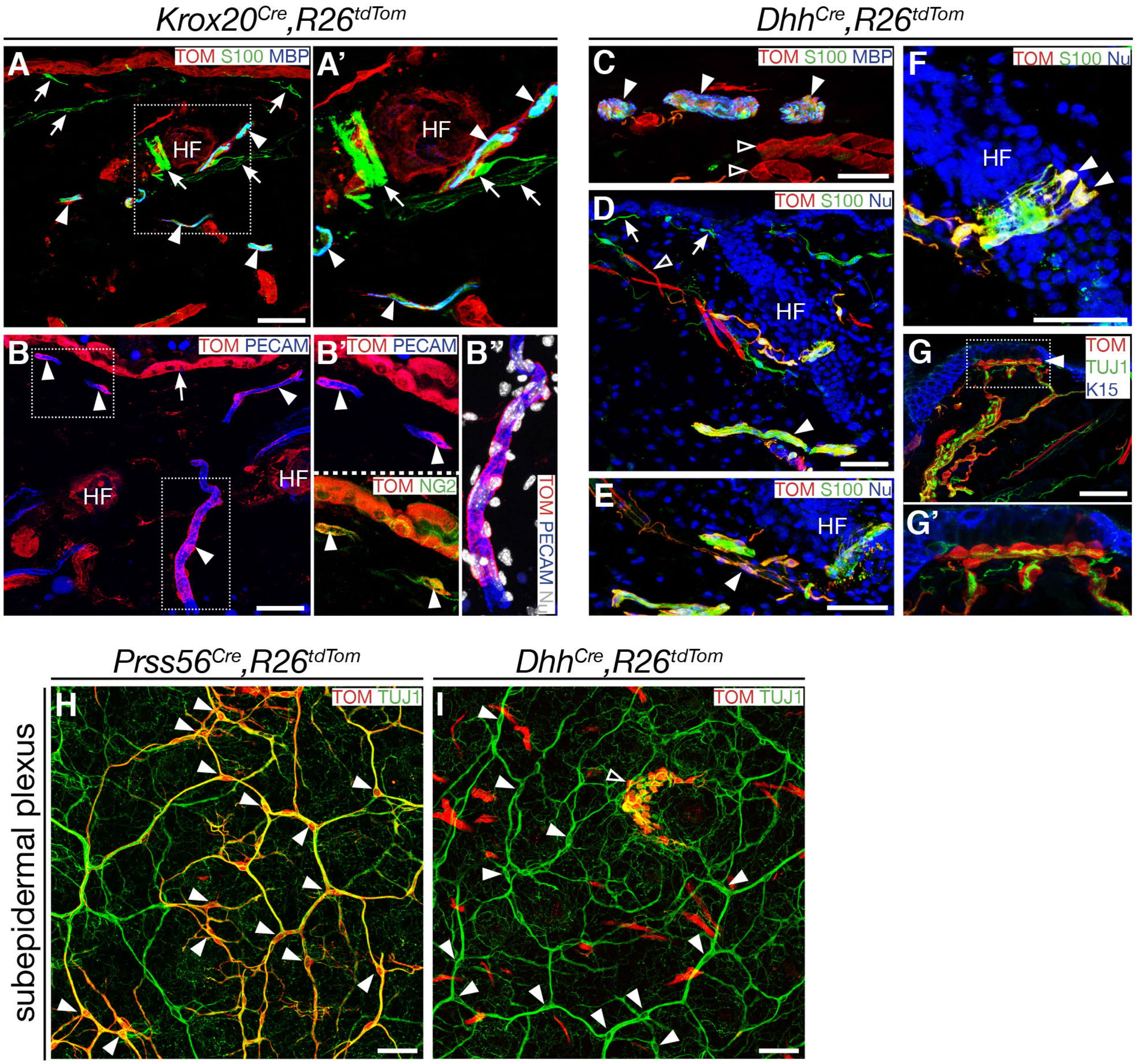

J

Cell type	*Prss56*^{Cre}	*Krox20*^{Cre}	*Dhh*^{Cre}
mSC	+	+	+
Remak SC	+	-	+
lanceolate glia	+	-	+
arrector pili glia	+	-	+
subepidermal glia	+	-	-
melanocytes	+	-	-
Merkel cells	-	-	+

Figure 7

Downloaded from http://aacrjournals.org/cancerdiscovery/article-pdf/doi/10.1158/2159-8290.CD-18-0156/2929956/2159-8290_cd-18-0156v1.pdf by guest on 20 October 2022